Ahmed Çağrı Sayın

A Masters. Thesis

AGU 2024

EXPERIMENTAL INVESTIGATION AND OPTIMIZATION OF CUTTING PARAMETERS TO MINIMIZE THE BURR FORMATION IN MILLING OF S2-GLASS FIBER REINFORCED PLASTICS

M.Sc. THESIS

SUBMITTED TO THE DEPARTMENT OF ADVANCED MATERIALS AND NANOTECHNOLOGY

AND THE GRADUATE SCHOOL OF ENGINEERING AND SCIENCE OF ABDULLAH GUL UNIVERSITY

IN PARTIAL FULFILLMENT OF THE REQUIREMENTSFOR THE DEGREE OFMASTER OF SCIENCE

By

Ahmed Çağrı Sayın

August 2024

EXPERIMENTAL INVESTIGATION AND OPTIMIZATION OF CUTTING PARAMETERS TO MINIMIZE THE BURR FORMATION IN MILLING OF S2-GLASS FIBER REINFORCED PLASTICS

A THESIS
SUBMITTED TO THE DEPARTMENT OF ADVANCED MATERIALS AND NANOTECHNOLOGY
AND THE GRADUATE SCHOOL OF ENGINEERING AND SCIENCE OF ABDULLAH GUL UNIVERSITY
IN PARTIAL FULFILLMENT OF THE REQUIREMENTS
FOR THE DEGREE OF
MASTER OF SCIENCE

By

Ahmed Çağrı Sayın

August 2024

SCIENTIFIC ETHICS COMPLIANCE

I hereby declare that all information in this document has been obtained in accordance with academic rules and ethical conduct. I also declare that, as required by these rules and conduct, I have fully cited and referenced all materials and results that are not original to this work.

Name-Surname: Ahmed Çağrı Sayın

Signature :

REGULATORY COMPLIANCE

M.Sc. thesis titled “Experimental Investigation and Optimization of Cutting Parameters to Minimize the Burr Formation in Milling of S2 Glass Fiber Reinforced Plastics” has been prepared in accordance with the Thesis Writing Guidelines of the Abdullah Gül University, Graduate School of Engineering & Science.

Prepared By	Advisor
Ahmed Çağrı Sayın	Asst. Prof Sinan Kesriklioğlu
Signature	Signature

Head of the Advanced Materials and Nanotechnology Program

Asst. Prof. Zeliha SORAN ERDEM

Signature

ACCEPTANCE AND APPROVAL

M.Sc. thesis titled “Experimental Investigation and Optimization of Cutting Parameters to Minimize the Burr Formation in Milling of S2 Glass Fiber Reinforced Plastics” and prepared by Ahmed Çağrı Sayın has been accepted by the jury in the Advanced Materials and Nanotechnology Graduate Program at Abdullah Gül University, Graduate School of Engineering & Science.

…….. /…….. / ……..

(Thesis Defense Exam Date)

JURY:

Advisor : Asst. Prof. Sinan Kesriklioğlu

Member : Asst. Prof. Çağatay Yılmaz

Member : Assoc. Prof. Şengül Danışman

Member : Asst. Prof. Mikail Temirel

Member : Asst. Prof. Farzin Mozafari

APPROVAL:

The acceptance of this M.Sc. thesis has been approved by the decision of the Abdullah Gül University, Graduate School of Engineering & Science, Executive Board dated ….. /….. / …….. and numbered ……..……. .

…….. /…….. / ……..

(Date)

Graduate School Dean

Prof. İrfan ALAN

ABSTRACT

EXPERIMENTAL INVESTIGATION AND OPTIMIZATION OF CUTTING PARAMETERS TO MINIMIZE THE BURR FORMATION IN MILLING OF S2-GLASS FIBER REINFORCED PLASTICS

Ahmed Çağrı Sayın
MSc. in Advanced Materials and Nanotechnology
Advisor: Assist. Prof. Sinan Kesriklioğlu
August 2024

Composite materials have a wide range of application areas due to their high mechanical properties, low density and versatility. Milling is an important process for the composite materials to shape them according to the needs of the application area. Burrs are often created during the milling process and result in rejection of parts in the desired usage area. This study focuses on the experimental and statistical analysis of the burrs during the milling process of S2-Glass Fiber Reinforced Plastics (S2-GFRP) and Basalt Fiber Reinforced Plastics (BFRP) composites. Damages occurring during the milling process were analyzed to evaluate the mechanical performance and surface quality of composite materials. Surface quality is determined by the area and length of the burrs that were produced during the milling operations. Optimum processing parameters have been determined to ensure minimum burr area and burr length. It is determined that there are multiple optimum parameters according to the processed material and cutting direction. Burr area and burr length are measured with image analysis. The total area of burrs is calculated, and the longest burr in each sample is measured. The effect of tool material, tool coating, spindle speed and feed rate on burr area and burr length is observed. Based on the experimental results, it was determined that the tool material is the only parameter that consistently affects burr area and bur length. The data obtained aims to ensure the more reliable and efficient use of these materials in engineering applications and makes significant contributions to sustainable production processes.

Keywords: S2-Glass Composite, Precision Milling, Coating, Image Analysis, Sustainable Manufacturing

ÖZET

S2-CAM ELYAF TAKVİYELİ PLASTİKLERİN FREZELENMESİNDE ÇAPAK OLUŞUMUNU EN AZA İNDİRMEK İÇİN KESME PARAMETRELERİNİN DENEYSEL İNCELENMESİ VE OPTİMİZASYONU

Ahmed Çağrı Sayın
İleri Malzemeler ve Nanoteknoloji Anabilim Dalı Yüksek Lisans
Tez Danışmanı: Dr. Öğretim Üyesi Sinan Kesriklioğlu
Ağustos 2024

Kompozit malzemeler yüksek mekanik özellikleri, düşük yoğunlukları ve çok yönlülükleri nedeniyle geniş bir uygulama alanına sahiptir. Frezeleme, kompozit malzemelerin uygulama alanının ihtiyaçlarına göre şekillendirilmesinde önemli bir işlemdir. Çapaklar genellikle frezeleme işlemi sırasında oluşur ve parçaların istenilen kullanım alanında reddedilmesine neden olur. Bu çalışma, S2-Cam Elyaf Takviyeli Plastik (S2-GFRP) ve Bazalt Elyaf Takviyeli Plastik (BFRP) kompozitlerin frezeleme işlemi sırasında oluşan çapakların deneysel ve istatistiksel analizine odaklanmaktadır. Kompozit malzemelerin mekanik performansını ve yüzey kalitesini değerlendirmek için frezeleme işlemi sırasında meydana gelen hasarlar analiz edildi. Yüzey kalitesi, frezeleme işlemleri sırasında oluşan çapakların alanı ve uzunluğuna göre belirlendi. Minimum çapak alanı ve çapak uzunluğunu sağlamak için optimum işleme parametreleri belirlendi. İşlenen malzemeye ve kesme yönüne göre birden fazla optimum parametrenin olduğu gözlendi. Çapak alanı ve çapak uzunluğu görüntü analizi ile ölçüldü. Çapakların toplam alanı hesaplandı ve her numunedeki en uzun çapak ölçülerek kayıt altına alındı. Takım malzemesi, takım kaplaması, takım devri ve ilerleme hızının çapak alanı ve çapak uzunluğu üzerindeki etkisi gözlemlendi. Deney sonuçlarına göre, takım malzemesinin, çapak alanı ve freze uzunluğunu tutarlı olarak etkileyen tek parametre olduğu belirlenmiştir. Elde edilen veriler, bu malzemelerin mühendislik uygulamalarında daha güvenilir ve verimli kullanılmasının sağlanmasını amaçlamıştır ve sürdürülebilir üretim süreçlerine önemli katkılar sağlaması beklenmektedir.

Anahtar kelimeler: S2-Cam Kompozit, Hassas Frezeleme, Kaplama, Görüntü Analizi, Sürdürülebilir İmalat

Acknowledgements,

I cannot emphasize how lucky I am to have Assistant Professor Sinan Kesriklioğlu. I am extremely thankful for his patience and guidance, so that in the end, I'm glad that I rejected a job offer from Japan to have a master's degree in AGÜ.

I also thank Assistant Professor Çağatay Yılmaz for providing the materials and the place for the project as the project leader, and his valuable guidance. I would also like to thank The Scientific and Technological Research Council of Türkiye (TUBITAK) for their financial support for the project within the framework of TUBITAK 1001 with the project code of 221M085.

I would also like to thank Associate Professor Şengül Danışman, Professor Kenan Danışman and Research Assistant Emin Ersoy for their valuable contributions for the coating process of the research.

I thank my family, my parents and my brother, for their valuable support.

TABLE OF CONTENTS

1. INTRODUCTION 1

1.1 An Overview to Composite Materials 1

2. MANUFACTURING OF S2-GFRP AND BFRP 8

2.1 Vacuum Infusion Process 8

3. CHARACTERIZATION OF COMPOSITES 12

3.1 Burn-out Test 12
3.2 Fiber Diameter Measurement 14
3.3 Mechanical Testing 17

4. COATING 18

4.1 Introduction to Coating 18
4.2 Magnetron Sputtering 18
4.3 Characterization of TiN Coatings 20

5. MACHINING OF COMPOSITES 26

5.1 Pre-Processing 26
5.2 Tool Preparation 28
5.3 Experimental Design 30
5.4 Machining 32

6. BURR ANALYSIS WITH IMAGEJ 34

6.1 Photography 34
6.2 Using ImageJ for Burr Area Measurement 34
6.3 Burr Length Measurement 37
6.4 Processing the Burr Area and Burr Length 38

7. STATISTICAL ANALYSIS 42

7.1 Signal-to-Noise (S/N) Ratio Analysis 42
7.1.1 Introduction to S/N Ratio 42
7.1.2 Signal-to-Noise Data 43
7.2 Analysis of Variance (ANOVA) 45
7.3 Desirability Analysis 49

8. CONCLUSIONS AND FUTURE PROSPECTS 54

8.1 Conclusions 54
8.2 Societal Impact and Contribution to Global Sustainability 55
8.3 Future Prospects 56

LIST OF FIGURES

Figure 1.1 Delamination types on a S2-GFRP sample 6
Figure 2.1 Assembly before the vacuum bag 9
Figure 2.2 Layout of the assembly 10
Figure 3.1 Weight measuring with a precision scale 13
Figure 3.2 Measurement of basalt fibers with a) 100X and b) 20X magnifications 14
Figure 3.3 Measurement of S2-Glass fibers with a) 20X and b) 100X magnifications 16
Figure 4.1 Magnetron sputtering system vacuum chamber 19
Figure 4.2 TiN thin film deposition and the schematics of characterization 20
Figure 4.3 a) Scanning Electron Microscopy (SEM) image of TiN coating on WC 10%Co, b SEM image of TiN coating on High-Speed Steel (HSS) and c Atomic Force Microscopy (AFM) analysis 22
Figure 4.4 X-ray diffraction patterns 24
Figure 4.5 Grain size of TiN thin films on substrates 25
Figure 5.1 a) AutoCAD drawing for the CNC code of the composites and b) the final product 27
Figure 5.2 BFRP (a) and S2-GFRP samples 28
Figure 5.3 Cutting directions and delamination of samples on the connecting piece ... 28
Figure 5.4 Manufactured tools that are a) helical carbide, b) helical HSS and c) straight carbide 29
Figure 5.5 a) Uncoated and b) coated end mills 30
Figure 5.6 Machining of a) BFRP and b) S2-GFRP samples 33
Figure 6.1 Applying color threshold with a) light directly on the sample, b) light is positioned in a way that the material casts a shadow below the burr 35
Figure 6.2 Burr measurement 36
Figure 6.3 Set Scale function in ImageJ 37
Figure 6.4 Burr length measurement with ImageJ 38
Figure 6.5 Burr area for conventional milling 38
Figure 6.6 Burr area for climb milling 39
Figure 6.7 Conventional burr length of S2-GFRP and BFRP 40
Figure 6.8 Climb burr length of S2-GFRP and BFRP 41

Figure 7.1 S/N ratio graphs for Burr area and burr length for a) conventional and b) climb milling of S2-GFRP 43
Figure 7.2 S/N ratio graphs for Burr area and burr length for a) conventional and b) climb milling of BFRP 44

LIST OF TABLES

Table 3.1 Material and mechanical properties of S2-GFRP and BFRP composite plates 16
Table 5. 1 Factors and levels in the experiments2 30
Table 5.2 Taguchi L18 parameter combinations3 31
Table 7. 1 ANOVA table for the burr area of S2-GFRP4 45
Table 7. 2 ANOVA table for burr length of S2-GFRP5 46
Table 7. 3 ANOVA analysis for the burr area of BFRP6 46
Table 7. 4 ANOVA analysis for the burr length of BFRP7 47
Table 7. 5 MRR with respect to the Taguchi parameter 49
Table 7. 6: Individual and composite desirability of the parameters for S2-GFRP9 50
Table 7.7: Individual and composite desirability of the parameters for BFRP10 51

LIST OF ABBREVIATIONS

ANN	Artificial Neural Network
ANOVA	Analysis of Variance
BFRP	Basalt Fiber Reinforced Plastics
CFRP	Carbon Fiber-Reinforced Plastics
CNC	Computer Numerical Control
CVD	Chemical Vapor Deposition
GFRTP	Glass Fiber-Reinforced Thermoplastics
MMC	Metal Matrix Composites
MRR	Material Removal Rate
PVD	Physical Vapor Deposition
S2-GFRP	S2-Glass Fiber-Reinforced Plastics
SG	Smart Grid

To my friends and family

Chapter 1

Introduction

In this chapter, an introduction regarding the importance and usage areas of composite materials will be done. The necessity of machining and optimization will be highlighted, and an overall literature review will be presented.

1.1 An Overview to Composite Materials

Composites are strong and lightweight materials. Products made with composites are resistant to corrosion caused by weather and chemicals and have a long service life. Composites can be molded into flexible and complex shapes, giving designers the freedom to create almost any shape or form. Compared to other materials, composites offer several advantages. Designers, engineers, and architects are replacing materials such as steel, aluminum, wood, and granite with composites due to the high strength, versatility, and low weight of composites. Composites are used in numerous markets including aerospace, architecture, automotive, energy, infrastructure, marine, military and sports and recreation. Researchers continue to find new ways to use composites to develop life-changing applications.

Most composite materials consist of two main parts: a reinforcement such as carbon fiber, glass fiber and basalt fiber, and a matrix for reinforcement to strengthen, such as epoxy and thermoplastics. There are many kinds of composite materials with various usage areas. Carbon fiber-reinforced plastic (CFRP) composites have applications in space-related industries, automotive, sports and marine industries due to their high tensile and fatigue strength, and low density [1]. Glass fiber-reinforced thermoplastics (GFRTP) composites show high damage tolerance and moisture resistance in order to be used in applications that requires high durability and high resistance to environmental factors [2]. Another variety of composite materials uses carbon nanotubes as a reinforcement. Jurn et al. (2020) used carbon nanotube composite materials in order to investigate their

application potential as terahertz antennas. Double-walled carbon nanotubes and bundle double-walled carbon nanotube composites demonstrates promise for high performance antenna systems [3]. Borosilicate glass fibers obtained from recycled materials shows high sustainability and low cost while having high corrosion resistance and variability [4] Metal matrix composites (MMCs) are extensively used in aerospace industry due to their high strength, fracture toughness and wear resistance. The composites are being used as aerospace components for enhancing the performance and durability [5]. Development of conductive polyaniline-coated poly(p-phenyleneterephthamide) yarn-reinforced multiaxial composites is proven useful in electromagnetic shielding while having significant electrical conductivity and mechanical properties, suggesting that the composite materials can be tailored and innovated on demand [6]. A study shows that boron carbide-titanium diboride composites have radiation shielding properties, showing diversity in applications. Polymeric composites with natural reinforcements have an increasing popularity in automotive industry due to their good mechanical and tribological properties. These composites provide a sustainable alternative to the common materials, and suitable for the applications that require high strength and durability [7].

Glass fiber reinforced plastics (GFRP) received significant attention due to their exceptional mechanical properties and applicational versatility. GFRP are manufactured by embedding glass fibers into a polymer matrix, having the properties of high thermal resistance and tensile strength [8]. GFRP has been used in a wide range of industries due to its versatility such as aerospace, construction, thermal insulation and marine industries [9]. Glass fiber-reinforced plastics are also known for their dimensional stability, highly affected by the fiber content inside the matrix. Research suggested that the glass fiber content affects the volumetric thermal expansion coefficient [10]. Glass fiber reinforced polypropylene is researched due to its light weight and durability to enhance the applications in the automotive industry [11]. Another research suggested the usage of GFRP in structural automotive applications, such as inductive charging systems inside the electric cars [12].

Glass fibers have a special method of naming, in order to simplify the classification of a wide range of materials. The naming method suggests that the initial letter of the designed area of the glass fiber must be used, followed by the -glass word. For example,

glass fibers that are suited for electrical insulation are named E-Glass, and the ones that are used for their high tensile strength are named S-Glass. The composition of the different glass fibers changes according to the desired usage area. An overview of the various members of the glass fiber family can be seen below: A-Glass (Alkali Glass): Refers to the glass fibers that contain alkali metals in their compositions (Li, Na, K, Rb etc.). The addition of alkali metals influences the mechanical properties of the glass fibers significantly by making the glass network more depolymerized [13]. Dielectric properties [14], physical and optical properties [15], electrical conductivity and mechanical properties of A-Glasses [16] are widely discussed in the literature.

AR-Glass (Alkali-Resistant Glass): A member of glass fiber family that is manufactured to withstand alkali environments. Various research suggested that the addition of zirconia (ZrO_2) to the glass fiber structure increases the alkali resistance of the material [17-19]. AR-Glasses are used to enhance the mechanical properties and alkali resistance of fiber-reinforced cement [20]

D-Glass (Dielectric Glass): Dielectric glasses are widely used in capacitors, memory devices and high-frequency dielectric materials. Borosilicate is used in the manufacturing of D-Glasses. Research suggests that the addition of rare-earth elements decreases the dielectric constant [21]. Dielectric properties of D-Glasses are examined under the high frequency to have a better understanding of their behavior [22].

E-Glass (Electrical Glass): Preferred for their good insulation properties. There are studies that discover alternative methods for manufacturing E-Glass fibers, such as powder metallurgy. The same research also focuses on optimizing the mechanical properties of E-Glass fiber-reinforced composites [23]. It is suggested that the addition of E-Glass to the composite systems increase the dielectric properties and thermal stability [24].

S-Glass (Structural Glass): S-Glass is a fiber with high tensile and compressive strength, high-temperature and impact resistance [25]. Due to its mechanical properties, S-Glass can be used in dental composites [26].

S2-Glass (Strength Glass): S2-Glasses have similar composition with S-Glass, with higher silica content. In literature fracture toughness on high strain rate impact response of thermoplastic polycarbonate-bonded S2-Glass/epoxy is investigated [27].

There are various methods for manufacturing composite materials. Vacuum infusion method is a widely used method for composite manufacturing. The method revolves around introducing resin to the fibers with the assistance of a vacuum, resulting in high quality composites [28]. The method utilizes a vacuum bag sealed over the selected fibers and vacuum ensures the homogeneity, lower void ratio, repeatability and strong mechanical properties for the resultant fiber reinforced composite material [29], [30].

An important advantage of the vacuum infusion method is that its ability to reduce the fiber and epoxy waste, increasing its cost-effectiveness [31]. The method is considered as the most cost-effective for damage-resistant airframe structures for carbon fiber-reinforced composites [32]. Additionally, the vacuum infusion method is considered as an attractive alternative for building large parts of materials while using easy-to-obtain tools, rendering the method easy to apply and versatile for various applications [33]. There are various studies for improving the efficiency of vacuum infusion method by enhancing the resin flow and distribution [34].

Manufactured composite materials often can't be used directly in the desired application. Milling is an important process to shape and refine composite materials, remove the excess resin, and achieve desired dimensional properties. Multiple studies for various composite materials aimed to optimize the milling process by researching the effects of milling on tool wear, surface roughness and delamination.

Surface roughness is an important parameter on composites due to its effect on the adhesion and bonding. The effect of machining parameters on surface roughness is widely discussed in literature. Kilickap et al. (2020) suggested an artificial neural network (ANN) in order to predict the effects of milling parameters on the surface damage. The researchers examined the effects of cutting speed, feed rate and the flute number of the end mills to the surface roughness of carbon fiber reinforced plastics (CFRP). They concluded that the optimum conditions for machining is with low feed rate and high number of flutes [1]. Xu et al. (2020) observed the effect of cutting parameters of a steel sample on the surface roughness in a similar fashion. Researchers used a nondominated sorting genetic algorithm II (NSGA-II) in order to optimize the machining process.

Tool selection is an important step of composite machining. Tools are often coated with thin films in order to improve their mechanical properties**.** Titanium-based coatings received significant attention combined with the sputtering method due to their mechanical and tribological properties [35-39].

Surface coatings are often used in tools in order to alter the surface properties of the tool and increase the machining performance. Researchers claimed that milling quality of GFRP is affected by the thickness and the type of the coating of the machining tool [40]. It is expected that the tools have very good mechanical properties, especially hardness and toughness [41]. TiN coating improves both aspects of the tools, making them more suitable for machining operations [38].

During the machining of a composite material, delamination is formed on the machined surface. According to Colligan and Ramulu [42], there are 3 delamination modes: “Type I delamination is a surface tearing, exposing uncut fibers; “Type II delamination identified as burr” – is uncut fibers without damage to the matrix or ply; and “Type III delamination appears as fuzzy” fibers attached to the machined surface [42, 43]. Of these, Type I delamination is the most studied. This type of delamination has a direct relationship not only with the fatigue life of the material but also with the ability of the material to work at long life cycles since it can reduce the material strength due to damage to the internal parts of the fibers and the structure, disturbing the tolerances of the connection between parts [44 - 47] In the aerospace industry, 60% of the rejection of parts is due to Type I delamination during drilling [48]. An image of S2-GFRP samples with the formation of various types of delamination can be seen in Figure 1.1.

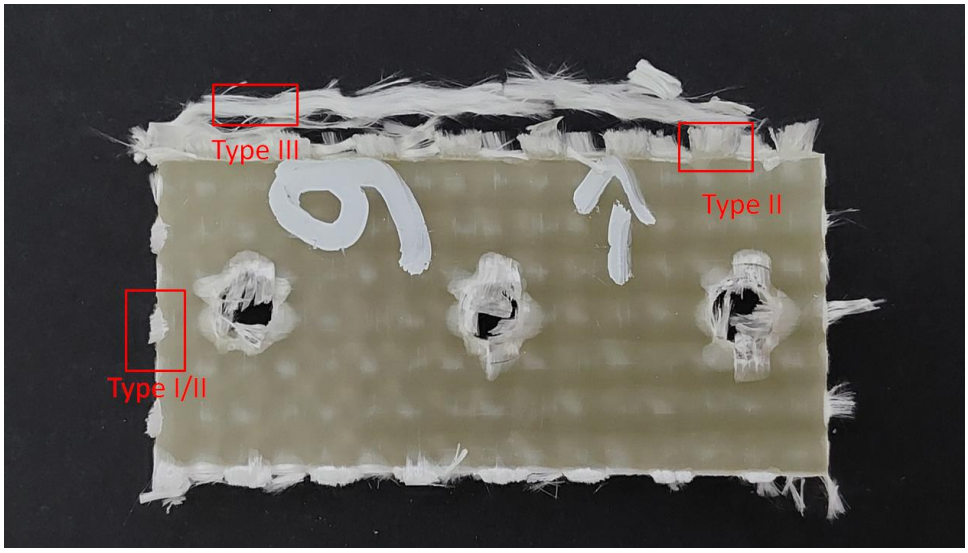

Figure 1.1 Delamination types on a S2-GFRP sample

Due to their heterogeneous structure, glass fiber-reinforced polymer (GFRP) composites present a number of complex challenges [48]. To optimize the machining process of composite materials, understanding the geometric (e.g., rake angle and helix angle) and cutting parameters (e.g., cutting speed and feed rate) is crucial [49]. Clearly, the efficiency of the milling process depends on the surface quality, tool life, cutting forces, and temperatures [43, 50]. The machinability of glass fiber-reinforced composites has been investigated to understand their effects on surface finish and tool wear [51]. Machining parameters such as cutting speed, feed rate, metal removal depth, and cutting tool surface properties are important factors affecting tool performance in the machining of composites. Sarma et al. [44] investigated the effect of cutting speed and depth of cut on the cutting force in GFRP pipes using a lathe with cubic boron nitride tools. The research group experienced combinations of feed rates of 0.048, 0.096, 0.143, 0.191, and 0.238 mm/rev and spindle speeds of 54, 82, 126, 194, and 302 m/min and concluded that low feed rates and high cutting speed were effective. Hocheng et al. [45] studied the effects of tool geometry of 10 mm diameter high-speed steel (HSS) drill bits on the delamination of carbon fiber reinforced composites. Among twist, saw, wax, core, and step drill bits, the research group suggested that the step drill is suitable for the highest feed rate operations with the least delamination. Jenarthanan and colleagues [46] proposed a mathematical model for milling-induced damage analysis in GFRPs. Among the combinations of cutting speed of 50, 100, and 150 m/min and feed rates of 0.10, 0.15, and 0.20, the group concluded that feed rate significantly increased the delamination

factor, while cutting speed had little effect on it. Kilickap [47] studied the drilling parameters in GFRP with cutting speeds of 10, 15, and 20 m/min and feed rates of 0.1, 0.2, and 0.3 mm/rev using a 5 mm cemented carbide tool. The researcher suggested that delamination around the hole increases with both cutting speed and feed rate.

Understanding composite materials and their structures requires in-depth knowledge of basic material behavior. Knowledge of fiber and resin behavior is essential to understanding the intricacies of composite manufacturing processes. This should be accompanied by stress, strain, and damage analysis in both static and fatigue regimes. Finally, designs must be produced and tested. Design optimization helps achieve the end goal is a successfully designed composite structure. In this context, the first step in realizing our project goal was to organize a suitable composite material laboratory donated with the necessary machinery and equipment. Therefore, we established our composite material laboratory in order to manufacture, research and experiment on composite materials.

Chapter 2

Manufacturing of S2-GFRP and BFRP

S2-glass fiber-reinforced plastic and basalt fiber-reinforced plastic samples that were used in the milling experiment were manufactured by implementing the vacuum infusion method. BFRP and S2-GFRP samples were produced by following this method. This chapter will focus on the details of the vacuum infusion method and steps that were taken in order to optimize the process.

2.1 Vacuum Infusion Process

The laboratory has all the materials required for composite plate manufacturing with vacuum infusion method. The steps for the vacuum infusion process are described.

Preparing the Infusion Table: Vacuum infusion table is prepared to the production by applying 4 layers of sealer and releaser. The sealer was first applied to a tissue, then the table was coated with sealer using the tissue. After 10 minutes, the process is repeated by applying a sealer to the tissue and then coating the table. After 4 repeats, the sealer layer was left to be cured for 30 minutes. The procedure was repeated with the same steps for releaser. Since both chemicals were hazardous for human health, latex gloves were used to handle the chemical-soaked tissue. Since the vapor of the chemical is also dangerous, laboratory was ventilated properly during the process.

Sizing: The fibers were cut in desired sizes. S2-GFRP samples were produced using 4 layers of S2-Glass fiber while BFRP samples were produced using 22 layers of basalt fiber. The desired size is expected not to be greater than 50cm in any dimension since a mistake in the process will result of more waste material, and overall harder to handle. Another reason is that the resin holder cups were standard in size, which is slightly less than a liter. It was possible to find suitable cups, however the progress was deemed unnecessary, and the production sizes were capped at 50cm in any dimension. Peel ply

and perforated film then cut into sizes that were slightly (2-3 centimeters) higher than the fibers, and infusion mesh is cut slightly lower than the fibers. Doing so allows the resin to flow through the material slower, giving sufficient time for infusion. A representation of the cut fibers and other required parts of vacuum infusion process before locking them with a vacuum bag can be seen in Figure 2.1.

Figure 2.1 Assembly before the vacuum bag

Assembly: In the production process of composite materials, different auxiliary materials are used to achieve the desired mechanical and surface properties. Among these auxiliary materials, peel ply, perforated film and flow mesh have an important place. Peel ply is a separator fabric used during surface preparation of composite materials. During the production process, the resin-coated composite is placed on the laminate and cured using vacuum bagging or autoclave methods. Once the curing process is complete, the peel ply is removed, and the composite surface becomes suitable for mechanical treatments or adhesion. This method is especially important in applications that require a second bonding process or painting because it does not leave any contamination or residue on the surface. Perforated film is used to ensure controlled expulsion of excess resin in composite production. It is placed on the composite laminate and directs the excess resin towards the vacuum bag thanks to its small holes. This helps the composite material maintain the ideal resin/material ratio, thus optimizing the mechanical properties of the material. Flow mesh is used to ensure even distribution of the resin throughout the

composite laminate. This network structure prevents the resin from reaching the entire laminate surface and creating gaps or dry areas. Flow mesh plays an important role, especially in the production of large and complex shaped composite parts, because it directs the flow of resin to ensure a uniform and homogeneous resin distribution. All these auxiliary materials work together to improve the manufacturing quality of composite materials, improve surface properties and optimize the performance of the final product. A vacuum bag sealant tape is applied to the circumference of the system with a rectangular pattern with 3-4 cm offset from the layout to fix the vacuum bag and the pipes. Sealant is heat resistant and has a dough-like texture which prevents air leakage. Resin inlet pipe and vacuum pipe are then fixed to the sealant tape, to the opposing edges of the rectangular. Depending on the size of the produced plate, leaving pockets on the vacuum bag is advised to prevent the over-stretching of the vacuum bag. Pipes are then locked to prevent the air from escaping the system. It is observed that even though the pipes are locked, the vacuum sometimes draws air from the locks, therefore a bit of sealant tape is applied to the tip of the pipes to prevent leakage. The assembly can be seen in Figure 2.2.

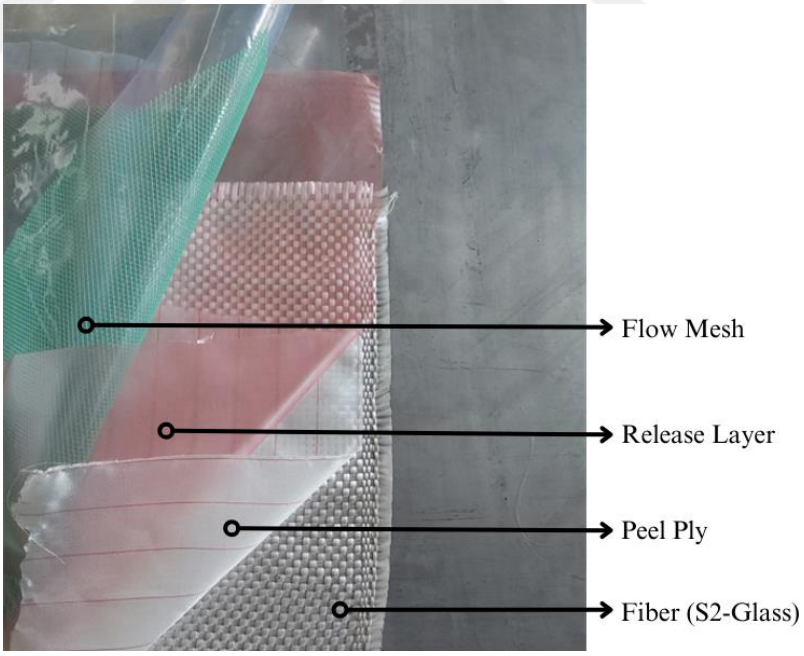

Figure 2.2 Layout of the assembly

Vacuum: The vacuum pump is started while the pipes are still locked. Then the valve between the vacuum chamber and the pump is opened, allowing the vacuum chamber to be vacuumed while the system is still locked. Then the lock is slowly removed, and vacuum is allowed to the system. The reason of releasing the lock slowly

is the risk of pipes and infusion mesh to damage the vacuum bag because of instantaneous pressure drop. It is expected that the system has leaks during this part. With the help of vacuum, the sounds from the leaks are tracked and sealed by applying pressure to the sealant tape. Leakage is often observed around the pipes; therefore, a double layer of sealant tape is used on the top of the pipes.

Leak Test: After all leaks are fixed, indicated by the absence of leaking sound, the pipes are sealed again to leave the system under the vacuum for 30 minutes, and the pressure in the vacuum chamber is noted. After 30 minutes, if there is a drop in the pressure more than 0.005 mmHg, it is considered that there is a micro-leak in the system, and the vacuum part is repeated. Else, the experiment continues without any problems.

Resin Preparation: Epoxy resin (Sika Biresin 122) and hardener (Sika Biresin 122.5) are mixed in a plastic holder with the measures of 100:30 by weight. It is advised to shake the hardener can before pouring it to the holder, since hardener may form heterogeneous layers after rest. The ingredients, epoxy resin and hardener, then mixed with the help of a wooden stick. After 5 minutes of mixing, the plastic holder is placed in the vacuum chamber.

Degassing: By applying vacuum to the vacuum chamber removes the gas bubbles from the epoxy resin/hardener mixture. It is observed that 10 minutes of exposure to vacuum is enough for degassing.

Finalization: The degassed resin is placed in the bottom of the infusion table and fixed with paper tape to the closest table leg. An empty plastic holder is placed in the vacuum chamber in order to collect the excess resin. The tape from the pipe is removed, and a pattern similar to a “beak” to the tip of the pipe is carved in with scissors. This prevents the pipe from sticking to the bottom of the resin holder due to vacuum. Then, the pipe is fixed to the plastic holder, preventing it from moving during the process. It is expected to observe resin to move through the pipe until the lock since the locks are not entirely air proof. Since the air that is supposed to be in the pipes is in the system due to lack of fastening of the locks, a couple more minutes of vacuuming is necessary to fully remove the air from the system. Then, both locks are removed, allowing resin to the system.

Chapter 3

Characterization of Composites

Required analysis for characterization of fibers and mechanical properties of the composite materials are done in this section. Burn-out test, fiber radius measurements and strength along with modulus of elasticity of the composites are determined according to the tests that will be explained in this chapter.

3.1 Burn-out Test

Burn-out testing is a testing method used to determine the proportion of resin or matrix material in composite materials. This test is based on the removal of the matrix material, usually polymer resin, in the composite by controlled burning or heating at high temperatures and measuring the remaining amount of fiber.

In order to determine the volume fraction, first, the rectangular shaped parts are cut off from the samples. The samples that were used in the machining couldn't be directly used in this experiment due to the holes on the composite samples. Therefore, a small rectangular portion of the samples are cut off from them and polished until the rectangular shape is obtained. 6 samples, 3 for each material, are prepared in this way for burn-out test.

The test begins with the precise weighing of the composite sample. The scale used in the experiment can be seen in Figure 3.1. At this stage, the total weight of the sample is recorded. The sample is then placed in a high-temperature oven and heated at high temperatures for a specified period. During this process, the matrix material that has a low burning point vaporizes, and only the fibers are left in the chamber. In this case after the recording of the first weight, the composite is burned inside an oven for 3 hours at 550 °C. Since the fumes from the epoxy could be toxic, the laboratory was ventilated properly during the experiment, and no one was present during the burning process. Once

the heating process is complete, the sample is removed from the oven and weighed precisely again. Since all the epoxy is now evaporated, only the weight of the fibers is measured. The weight of the epoxy matrix can be easily calculated by subtracting the weight of fibers from the initial weight.

Burn-out testing is widely used to determine the fiber volume fraction and matrix ratio contained in composite materials. This information is critical to understanding the mechanical properties and performance of composite materials. Especially in areas requiring high performance such as the aerospace, automotive and defense industries, accurate determination of material composition is of great importance in terms of reliability and quality control.

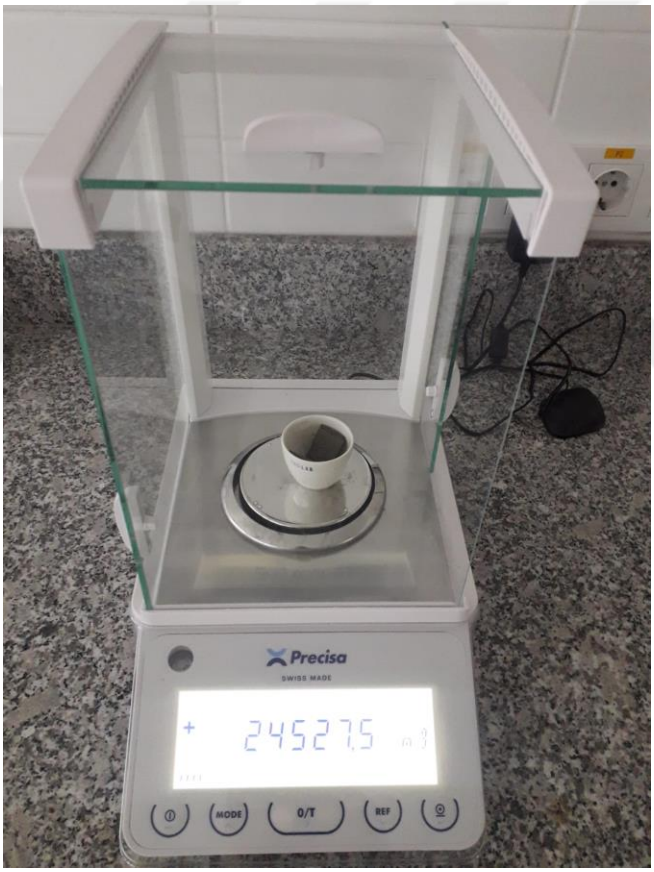

Figure 3.1 Weight measuring with a precision scale

3.2 Fiber Diameter Measurement

In order to measure the diameter of fibers, a Zeiss Gemini Axio Imager M2 model optical microscope and its integrated distance measurement function is used. Multiple measurements are taken from the various fibers for each sample. The microscope images of basalt fibers can be seen in Figure 3.2.

a)

b)

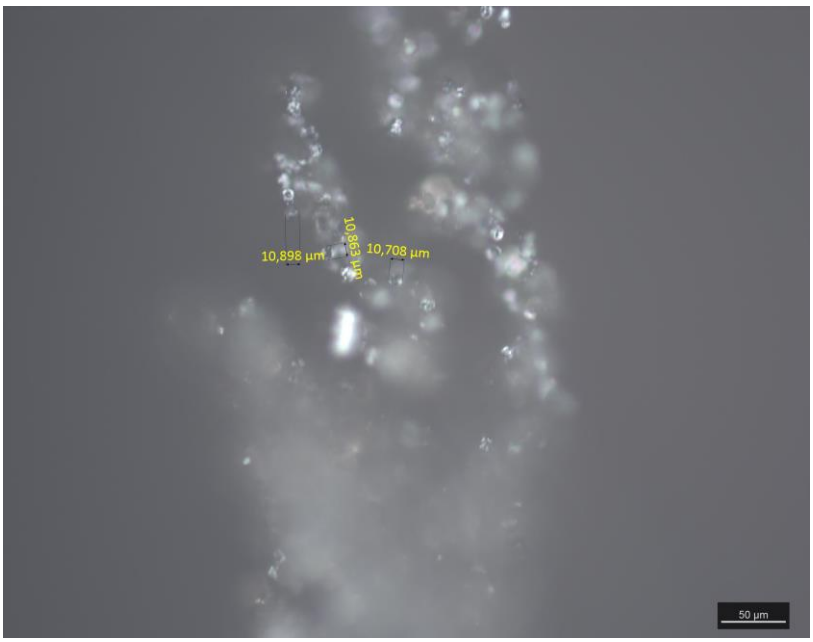

Figure 3.2 Measurement of basalt fibers with a) 100X and b) 20X magnifications

Similarly, microscopy image for the S2-Glass fibers can be seen in Figure 3.3. Photography of the fibers are done in different magnifications in order to double-check the results. The measurements are done from the fibers directly, instead of grinding and polishing of a composite sample.

a) 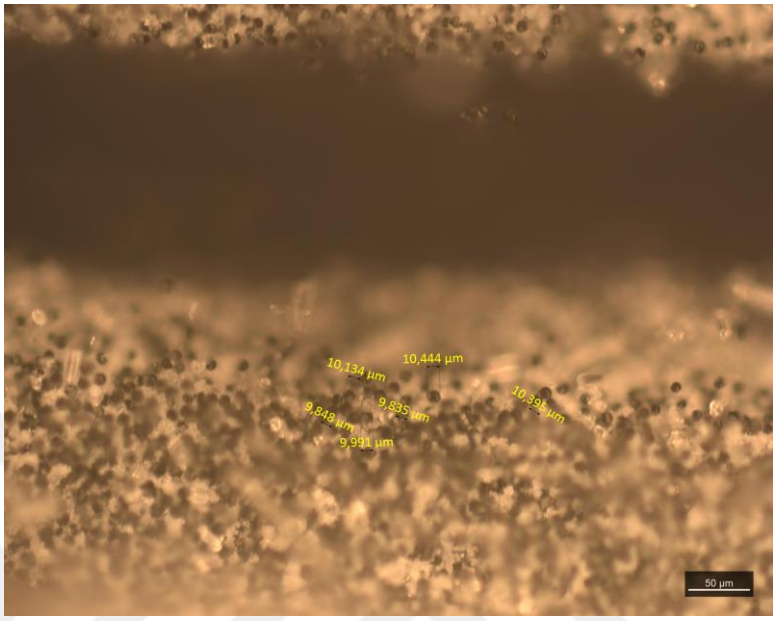

b)

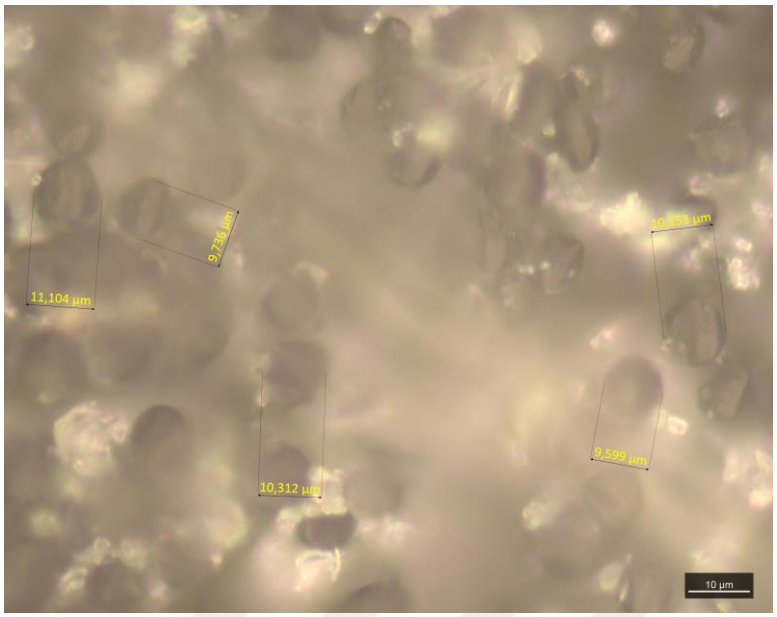

Figure 3.3 Measurement of S2-Glass fibers with a) 20X and b) 100X magnifications

3.3 Mechanical Testing

Instron 8801 tensile test setup is used for the mechanical testing of composite samples. Samples were prepared according to the ASTM 3039 standards, and tensile strength along with modulus of elasticity of the samples are measured. All of the characterization data is gathered into a single table, shown in Table 3.1.

Table 3.1 Material and mechanical properties of S2-GFRP and BFRP composite plates

Material	Young's Modulus (GPa)	Tensile Strength (MPa)	Fiber Diameter (μm)	Layers of Fibers	Fabric GSM	Weave Type	Fiber Volume Fraction
BFRP	18.88	487	10	22	220	Plain	47%
S2-GFRP	19.87	588	11	4	800	Plain	59%

Chapter 4

Coating

In this section, titanium nitride (TiN) coating and characterization of coating will be discussed. An overview of PVD and magnetron sputtering methods will be given and the characterization of the thin-film coating along with the methods of characterization will be discussed.

4.1 Introduction to Coating

Chemical Vapor Deposition (CVD) and Physical Vapor Deposition (PVD) are two of the most common methods for tool coating. CVD utilizes chemical vapors that decompose into a solid film as a substrate, while in PVD the solid material is vaporized inside a vacuum chamber, then condenses into the material in a form of a thin film. The literature shows that tools coated with PVD performs better and results with smoother surface compared to the tools coated with CVD [41] Among these two methods, PVD has a specialized method of precision coating, namely magnetron sputtering.

4.2 Magnetron Sputtering

Magnetron sputtering process usually consists of multiple steps and parts that the steps are taking place. Vacuum chamber is the main part of the magnetron sputtering that the coating takes place. In order to direct the PVD inside the vacuum chamber, the chamber has to be free of any other gaseous media. The vacuum chamber used in this experiment can be seen in Figure 4.1.

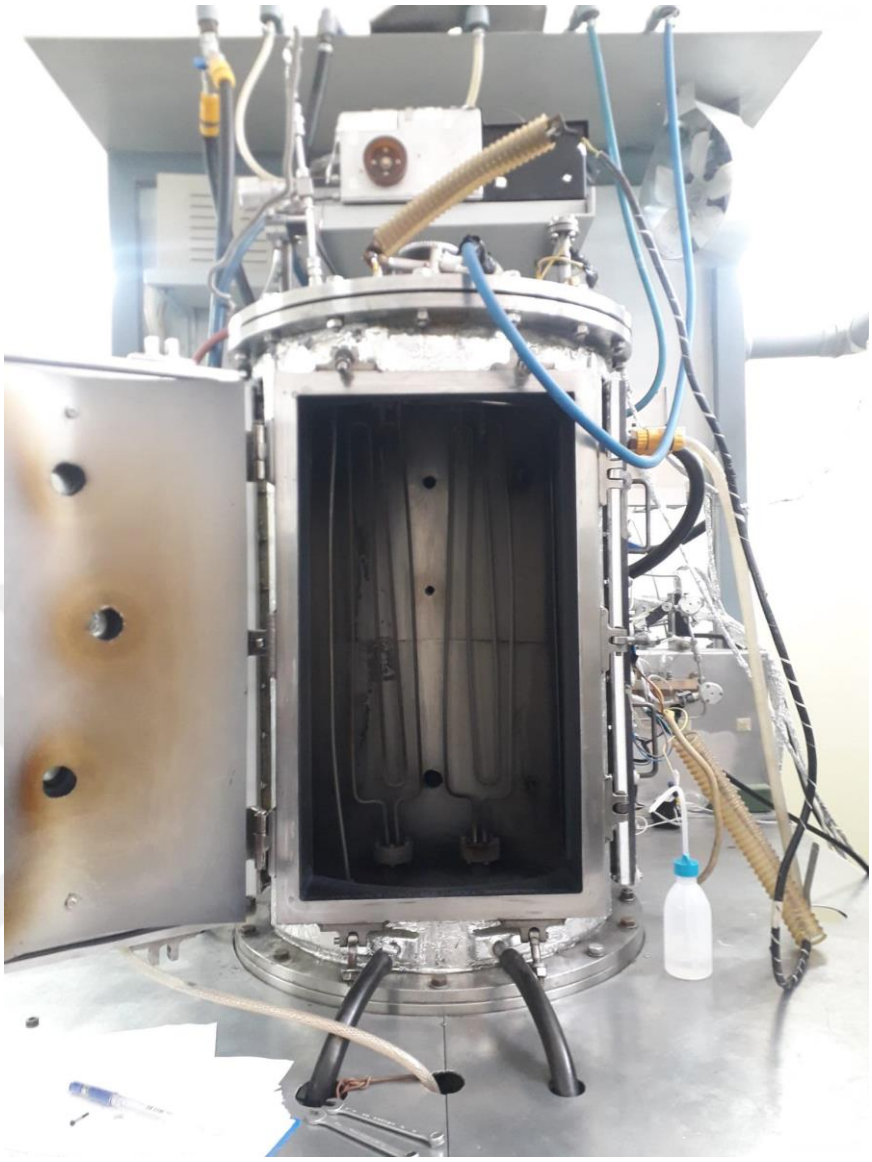

Figure 4.1 Magnetron sputtering system vacuum chamber

Magnetron sputtering process is based on a target material that is to be deposited as a thin film. The process starts with cleaning the material that will be coated to prevent any contamination to prevent the adhesion of the metal ions. Clean samples are inserted to the vacuum chamber, then vacuum is applied to the system. Later, gases such as argon or nitrogen is introduced to the system that is under vacuum for the purpose of creating plasma with the application of a high voltage. The voltage later forms a glow discharge. The positively charged ions are attracted to the negatively charged target, accelerated and hits the target to eject the ions from the target. For this research, titanium target is used, therefore the ejected ions are titanium ions. The ion ejection process is called “sputtering”. The sputtered ions then travel through the vacuum and condense on the object that needs

to be coated, in this case, CNC tools. The coating is then characterized by various methods such as EDX, SEM, AFM and visual inspection to determine elemental composition, roughness and any impurities that may have been formed during the process. The visualization of the process can be seen in Figure 4.2.

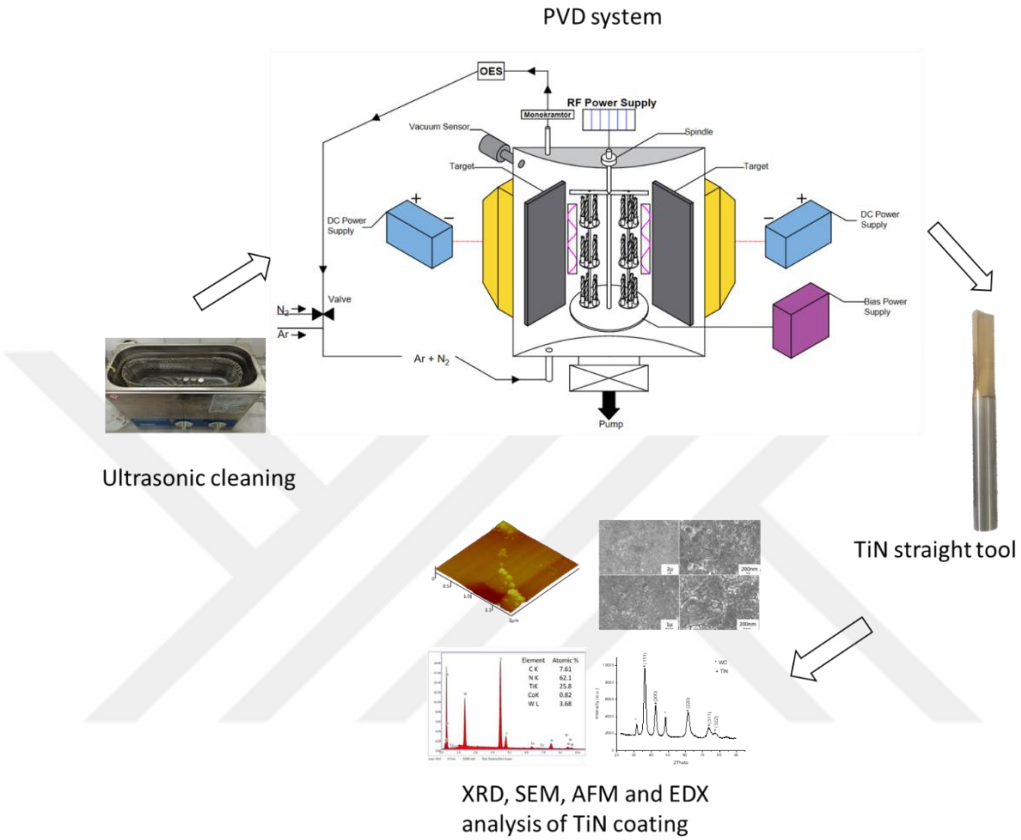

Figure 4.2 TiN thin film deposition and the schematics of characterization

4.3 Characterization of TiN Coatings

Coating process parameters such as target power, reactive gas ratio and working gas pressure are of great importance in determining the microstructure of thin films. Factors such as film density, grain size and thickness are affected by these parameters and ultimately determine the film properties. Therefore, control of these coating parameters allows the thin film microstructure and properties to be tailored to application needs.

Figure 4.3 shows the microstructure and surface morphology of the titanium nitride (TiN) coating layer. In Figure 4.3, SEM images taken at different magnifications highlight the TiN coatings on WC-10%Co and HSS-E substrates. In the HSS-E substrate (Figure 4.3a), the TiN surface exhibits distinct grain boundaries, pores, and voids. In contrast, TiN in the WC-10%Co substrate shows a denser, uniform cauliflower-shaped structure (Figure 4.3b). The TiN layer was observed in high integrity without discontinuities. Furthermore, AFM analysis reveals that the surface of the TiN film layer is smooth but contains bumps in places (Figure 4.3c). Chun et al [52] observed similar surface features related to coating parameters. The observed differences in thin TiN films obtained on different substrates under the same process parameters highlight an important effect.

a)

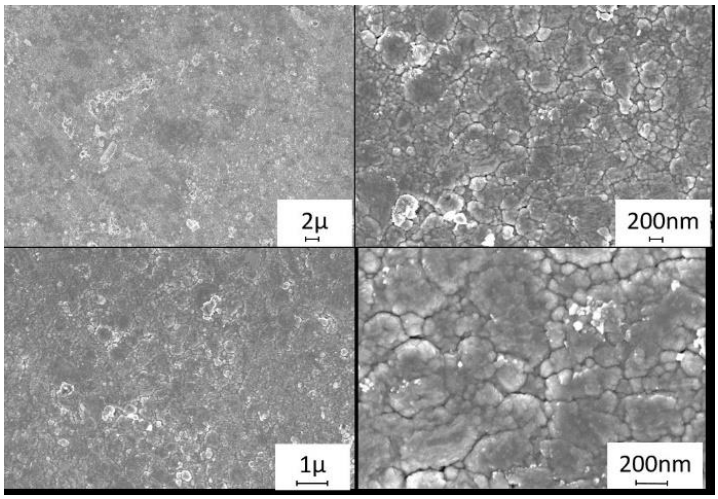

b)

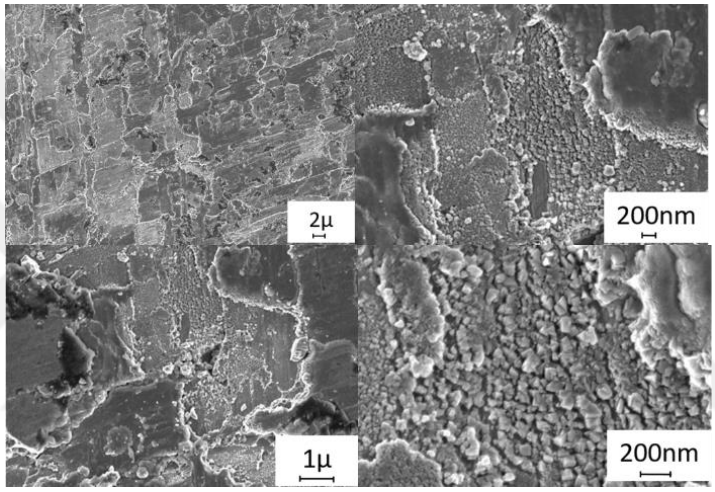

c)

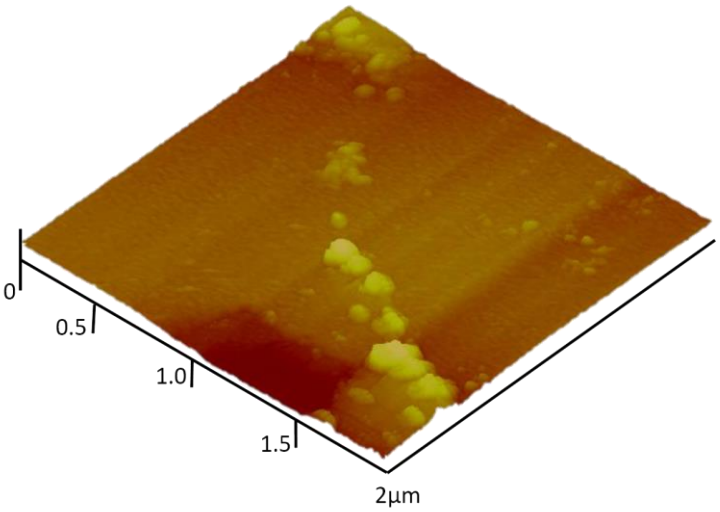

Figure 4.3 a) Scanning Electron Microscopy (SEM) image of TiN coating on WC 10%Co, b SEM image of TiN coating on High-Speed Steel (HSS) and c Atomic Force Microscopy (AFM) analysis

Nitrogen atoms located in the lattice spaces in the microstructure significantly affect the hardness of TiN thin films. The presence of nitrogen and titanium detected by EDX analysis confirms the formation of the TiN coating with the determined N and Ti atomic percentage values. Considering that TiN coating is applied to milling tools, its hardness plays an important role in operational performance. As a result of the hardness tests performed using the CSM Instrument brand nano hardness tester, hardness values of 2238 HV and 1672 HV were measured for WC-10%Co and HSS-E coatings, respectively. The relatively lower hardness of HSS-E thin films can be attributed to both grain size and voids in the film morphology. The influence of grain sizes and voids on the overall hardness properties is emphasized. Surfaces with micro-voids generally show lower hardness values. The bias voltage applied during plating also affects hardness; Therefore, it is important to determine the critical bias voltage [53, 54] High bias voltage increases the compressive stresses within the film, leading to a decrease in nanohardness due to residual stresses [55]. X-ray diffraction patterns of TiN thin films were analyzed, and TiN (111), (200) and (220) planes showed the most intense peaks. As can be seen in Figure 4.4, the analysis results (JCPDS-ICOD: 38-1420) confirmed the compatibility with TiN. In particular, TiN (111) emerged as the most dominant peak in thin films sputter-coated in a DC magnetic field[54]. When the TiN (111) texture on all substrates was examined, it was observed that it showed a distinct peak characteristic, consistent with the literature indicating a preferred orientation. Additionally, the increase in Ar content in the plasma environment has been associated with the increase in (111) orientation [38].

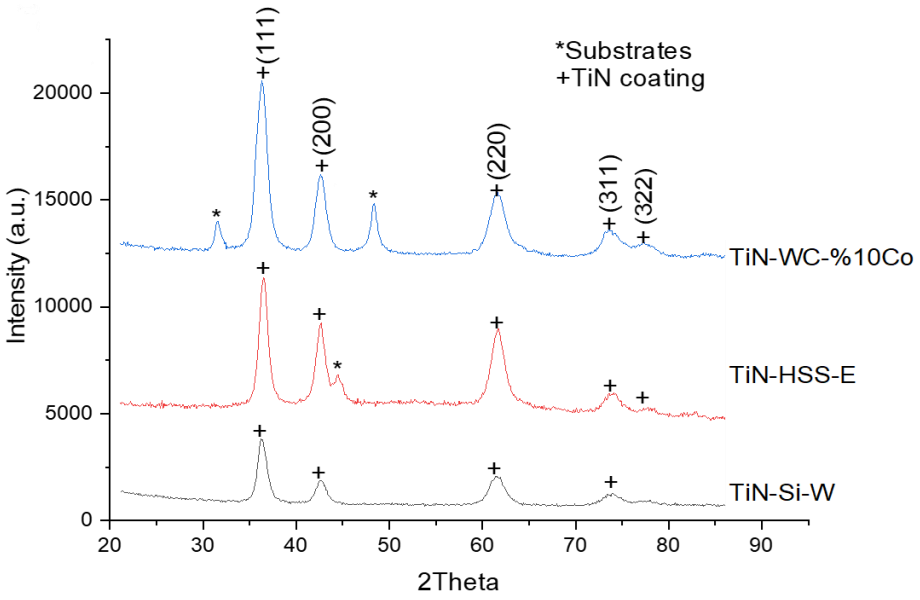

Figure 4.4 X-ray diffraction patterns

The Scherrer formula is an equation used to calculate the average size of crystals using X-ray diffraction, taking into account the amount of expansion of crystals in width (half-maximum width). This formula is especially used in determining small crystallite sizes such as thin films and nano-sized crystals. The Scherrer formula is as follows:

$$D = \frac{0.9x\lambda}{\beta x Cos\theta} \tag{4.1}$$

where D is the crystallite size (in nanometers), λ is the X-ray wavelength, β is the half-maximum width (in radians) of the diffraction line and θ represents the Bragg angle (central angle of the diffraction peak). The wavelength of the X-ray source is usually in Angstroms (Å) or nanometers (nm), common wavelengths used in diffraction experiments. The width of the diffraction peak varies depending on the size of the crystal; smaller crystallites have broader diffraction peaks. This formula is an important tool in the study of the microstructure of materials and the characterization of their nanoscale structures. Crystallite size of the TiN thin film coatings can be seen in Figure 4.5

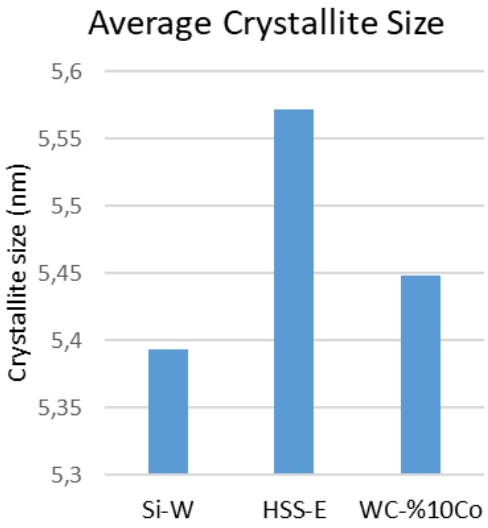

Figure 4.5 Grain size of TiN thin films on substrates

Crystallite size calculations made with the Scherrer formula revealed finer grain sizes in the WC-10%Co substrate compared to HSS-E. This result explains the superior hardness observed in hardness tests of TiN coatings deposited on WC-10%Co substrate.

Coated cutting tools have a significant impact on surface roughness and cutting forces depending on cutting parameters. It has been observed that increasing the cutting speed by using TiN-coated carbide tools in the processing of CRFP samples causes an increase in surface roughness. A surface roughness of 3.2 micrometers, considered high for aerospace applications, was recorded at a cutting speed of 100 mm/min and a feed rate of 0.25 mm/tooth [56]. The fact that TiN-coated tools showed a negligible effect on the burr area can be attributed to the surface treatment effect. The findings highlight the important role of feed rate as one of the most important factors affecting surface roughness in the machining of composite materials [57]. Therefore, it is imperative to meticulously analyze both cutting parameters and tool geometry for each composite material. Considering the different nature of the milling process of composite materials from other materials [40], this study examined both coated and uncoated tools.

Chapter 5

Machining of Composites

In this chapter, pre-processing, experimental design, and machining of the composites are explained in detail. Further details regarding the tools are given. Experimental design and the implementation of Taguchi method to the design and machining parameters and their significances are discussed. The machining process using a CNC lathe will be explained in detail.

5.1 Pre-Processing

Produced composite plates were first machined into 40 mm x 70 mm plates using Hannsa YL1000B CNC lathe, and a 6 mm pyramid tool specialized to machine composites. Nails with the size of 6 mm were left on the plates in order to ensure the stability of the plate and reduce chattering during the machining process. Three holes were drilled into each plate. The holes were then used to fix the plates to the CNC table using a 3D-printed connection part.

The drawing of the samples was made in AutoCAD, then translated into G-Code for the CNC lathe to read. Spindle speed and feed rate values were manually updated in the code, set to 1000 rev/min and 0.1 mm/rev respectively. The AutoCAD drawing and resulting plates can be seen in Figure 5.1.

a)

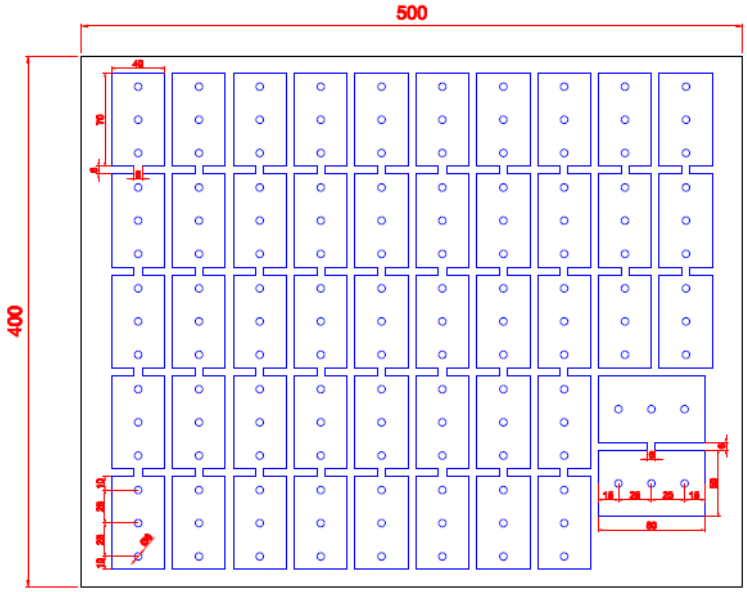

b)

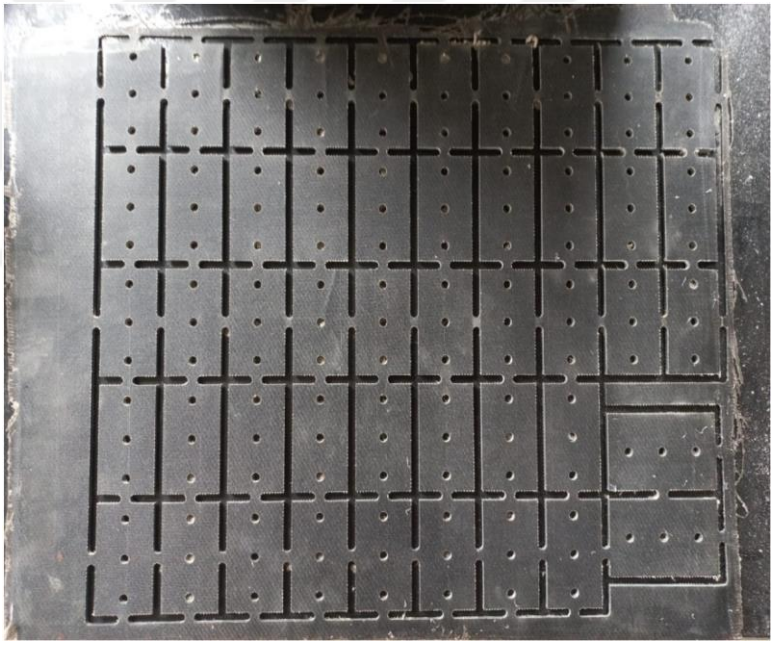

Figure 5.1 a) AutoCAD drawing for the CNC code of the composites and b) the final product

The plates are then separated from the nails using a handsaw, then preprocessed in CNC to chip out the excess material from the removal of nails. Cleanly machined samples from both materials can be seen in Figure 5.2.

a) 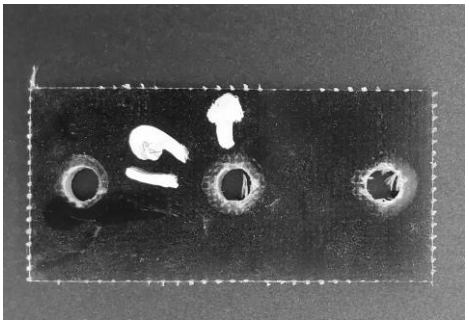 b) 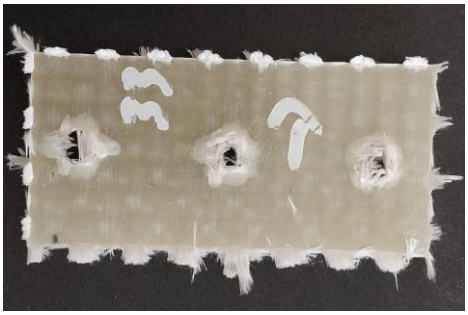

Figure 5.2 BFRP (a) and S2-GFRP samples

After the separation of plates, the plates were fixed to the composite using the connection tool. Figure 5.3 clarifies the cutting directions on the samples during the machining.

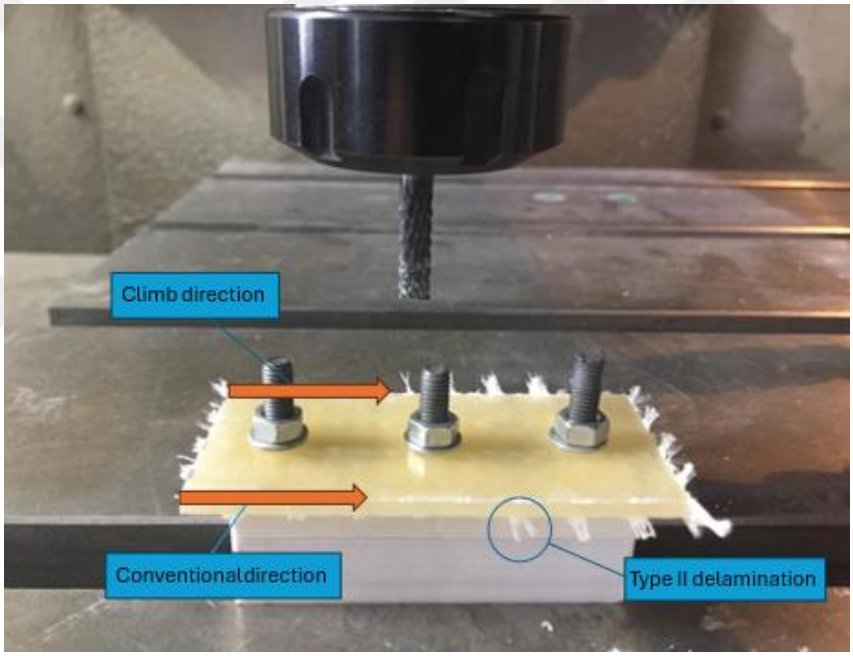

Figure 5.3 Cutting directions and delamination of samples on the connecting piece

5.2 Tool Preparation

10 carbide rods with the length of 330mm, H6 tolerance and with the quality of BS710 (HB10F) are bought from an external supplier, Boehlerit. The rods are then cut into 4 equal parts with 82.5mm length. A 10mm 2 flutes high-speed steel (HSS) tool was bought from an external supplier. A carbide tool is modelled after the HSS tool with the exact same geometry, flute number and angles. Therefore, a comparison between a

carbide tool and a HSS tool can be made without considering the effect of geometry. The modelling of the tool and cutting of carbide sticks are done in Kayseri 2nd Air Supply and Maintenance Center Command. A straight-flute carbide tool was also modelled from the carbide sticks to observe and compare the effects of geometry. Visualization of the tools before coating can be seen in Figure 5.4.

a) b) c)

Figure 5.4 Manufactured tools that are a) helical carbide, b) helical HSS and c) straight carbide

The tools were then coated to observe the effect of coating on the burr length and burr area, according to the explanations that were given in Chapter 4. The tools with the coated counterparts can be seen in Figure 5.5.

a)  b) 

Figure 5.5 a) Uncoated and b) coated end mills

5.3 Experimental Design

Experimental design of machining process was a challenge due to the high number of parameters that need to be controlled. The parameters, being spindle speed, feed rate, coating, cutting direction, tool geometry and tool material, are fundamental for the research. Spindle speed is the speed that the milling tool rotates, and the unit was chosen to be rev/min. The experiments were designed to assess the measures of spindle speed of 500, 1000 and 1500 rev/min. Feed Rate is the speed that the tool moves in the chosen direction. The unit is determined to be millimeter per revolution of the tool (mm/rev). Coating refers to whether the tool is coated with the TiN or not. Three different types of tools were used in the experiment. Two of them are made from the same carbide material while having different geometries, namely helical and straight, and the other one is made from HSS and have helical geometry. Cutting direction is also considered. Conventional and climb milling are two primary milling directions that can significantly impact the machining process. In conventional milling, the cutter rotates against the direction of feed, while in climb milling, the cutter rotates in the same direction as the feed. Cutting direction is not one of the Taguchi parameters, however the whole experimental setup was done for both cutting directions separately. Taguchi table of factors and levels can be seen in Table 5. 1.

Table 5. 1 Factors and levels in the experiments

Parameters	**Level 1**	**Level 2**	**Level 3**
Tool Surface	Uncoated	Coated	-
Tool Type	Helical Carbide	Straight Carbide	Helical HSS
Cutting Speed [rev/min]	500	1000	1500
Feed [mm/rev]	0.050	0.100	0.150

The table consist of combinations of factors and levels that were determined in Table 5. 1 . The Taguchi L18 orthogonal array arranges the levels and parameters into a unique combination (Table 5.2), so that the required number of experiments to determine the optimum parameters are less than trying every single parameter combination.

Table 5.2 Taguchi L18 parameter combinations

Experiment No.	Coating	Tool Type	Spindle speed	Feed rate
1	Uncoated	Helical Carbide	500	0.05
2	Uncoated	Helical Carbide	1000	0.1
3	Uncoated	Helical Carbide	1500	0.15
4	Uncoated	Straight Carbide	500	0.05
5	Uncoated	Straight Carbide	1000	0.1
6	Uncoated	Straight Carbide	1500	0.15
7	Uncoated	Helical HSS	500	0.1
8	Uncoated	Helical HSS	1000	0.15
9	Uncoated	Helical HSS	1500	0.05
10	Coated	Helical Carbide	500	0.15
11	Coated	Helical Carbide	1000	0.05
12	Coated	Helical Carbide	1500	0.1
13	Coated	Straight Carbide	500	0.1
14	Coated	Straight Carbide	1000	0.15
15	Coated	Straight Carbide	1500	0.05
16	Coated	Helical HSS	500	0.15
17	Coated	Helical HSS	1000	0.05
18	Coated	Helical HSS	1500	0.1

Each experiment repeated 3 times for both conventional and climb milling directions. Signal-to-noise ratio analysis is done according to the results. The data is discussed in Chapter 7.

5.4 Machining

A CNC mill (Hannsa YL1000B) is used to machine the composite samples. Suitable protection is used in order to not get exposed to the glass and basalt dust during the operation. Cutting parameters were changed inside the G-Code according to the Taguchi parameters. The machining of S2-GFRP and BFRP can be seen in Figure 5.6.

a)

b)

Figure 5.6 Machining of a) BFRP and b) S2-GFRP samples

Chapter 6

Burr Analysis with ImageJ

In this chapter, burr area and burr length calculation steps will be discussed in detail. Explanations regarding the usage of the ImageJ program will be given, and the overall process of image analysis using the program will be explained in detail. The obtained data for burr area and burr length will be discussed and optimum parameters for burr area will be obtained from the data.

6.1 Photography

The samples are photographed by a camera integrated to Samsung S7 FE model tablet. The properties of the camera are 8MP Sony IMX355 with a 28mm lens. During the photography, the camera is consistently held 10cm away from the samples in a stable surface to prevent shaking and focus related distortions.

6.2 Using ImageJ for Burr Area Measurement

ImageJ program is used to “highlight” the elements in the photograph that have different color than the others. Adjust threshold is the most critical function of this analysis. Depending on the adjusted color threshold, the highlighted area changes. Pixel to mm^2 conversion is made within the ImageJ program.

Since the burrs usually have different colors, it is easy to set the color threshold to only cover the burrs. However, there are times that are due to shadow and light parameters. When the light is set accordingly, it is possible to set a higher contrast difference between the surface that the samples are photographed and the burrs. An example of the effect of shadow can be seen in Figure 6.1.

a)

b)

Figure 6.1 Applying color threshold with a) light directly on the sample, b) light is positioned in a way that the material casts a shadow below the burr

Figure 6.1 shows that putting the light in a way that casts a shadow increases the accuracy of the analysis, however the effect it adds is ignorable and it is hard to standardize a method with the same lighting every single time. As it can be seen in Figure 6.1b, the burr has sharper tone difference and is highlighted better, however as the burr gets closer to the composite, the shadows somehow interfere with the program, and the highlighting efficiency decreases. In this study, light is held from the side of the burr consistently to obtain the Figure 6.1a every single time.

A highlighted surface for a glass sample can be seen in Figure 6.2. The figure appears completely highlighted due to the lack of contrast difference between the burr (white) and the composite sample (yellow). In order to standardize the measurement of burrs, a custom rectangular shape on the top side of Figure 6.2 is used, and only the area that has burrs covered by it is measured. For the other side of figure, the shape is turned 180° and the burr area is measured in the same way.

Figure 6.2 Burr measurement

The custom rectangular has 5 mm offset from each side of the composite sample. The reason is, as it can be seen in Figure 6.2 and Figure 6.3, the corner of the composite samples tends to produce excessive burr. However, the burr formed this way is not consistent and does not occur every single time, and its size and position are chaotic. Therefore, the offset is applied to each side to prevent the corner burrs from interfering with the total burr area calculations.

The program calculates the percentage of areas highlighted in the rectangular shape. Therefore, several steps need to be taken in order to ensure the conversion process takes place smoothly.

Set Scale Function: The app allows the user to set a distance with a line and calculates the length of the line in pixels. For this example, the known distance reference length is measured as 67.2 mm. ImageJ then calculates how many pixels are there for each unit of length given and uses it as a scale. When the “global” setting is ticked, the scale is set for all the samples that will be analyzed during the session. A usage of Set Scale function can be seen in Figure 6.3.

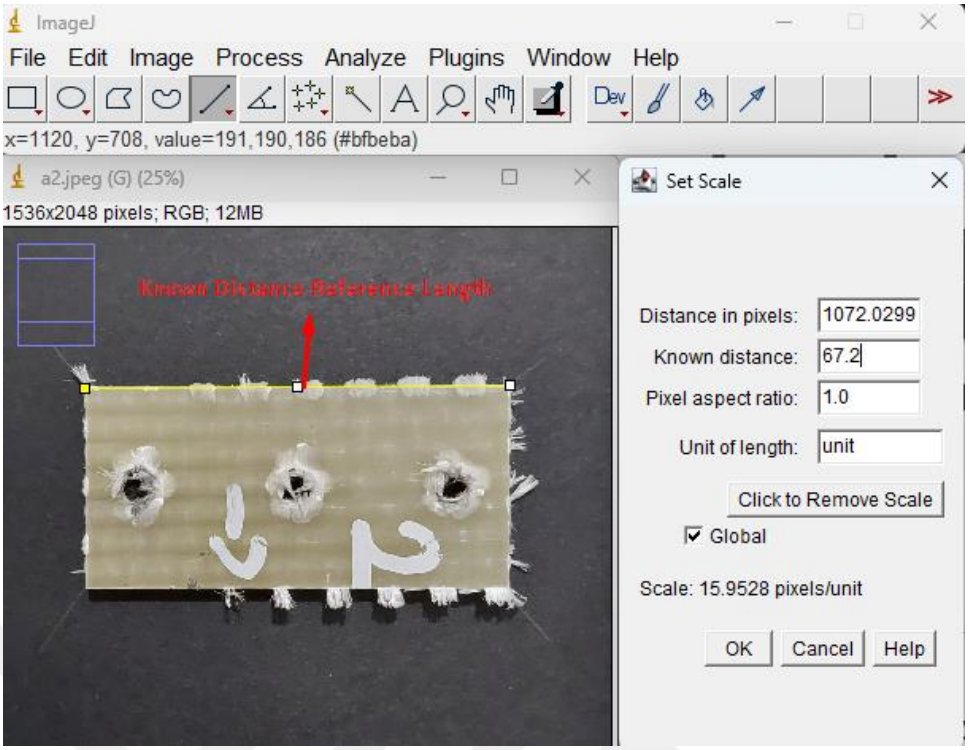

Figure 6.3 Set Scale function in ImageJ

Area Calculation: The app calculates the percentage of highlighted area inside the drawn shape, which in this case, the custom rectangle. The app also calculates the total area covered by the shape. By knowing these two parameters, it is possible to calculate the burr area according to the formula:

$$Burr\ Area = \ Area\ of\ Shape * Highlighted\ Area/100 \qquad (3.1)$$

The unit of the resultant area is pixel². To convert it to mm², it is simply multiplied by the scale calculated by set scale function.

6.3 Burr Length Measurement

Burr length is measured in a similar fashion to burr area measurement. Longest burrs are defined and measured in every sample. The burrs that are formed around the corners are excluded from this measurement, only the burrs in the area defined by the custom rectangular in Figure 6.4 is measured. The measurement of burrs is done with a 90° angle from the composite samples and the same scaling parameter is used for both length and area measurements.

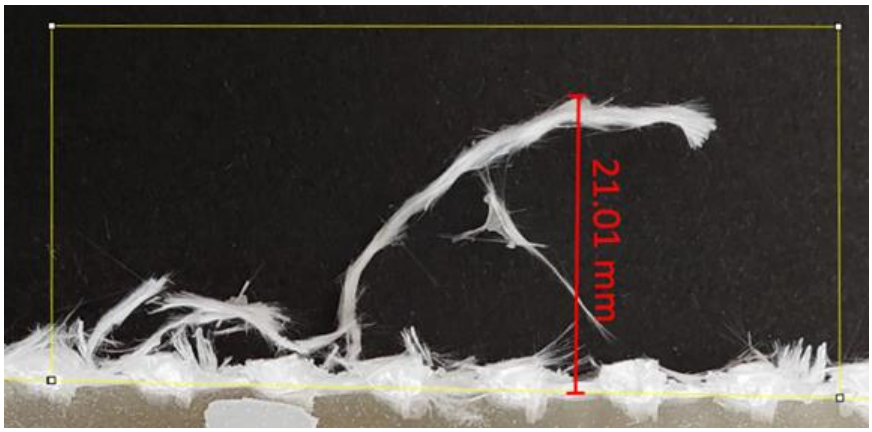

Figure 6.4 Burr length measurement with ImageJ

6.4 Processing the Burr Area and Burr Length

Mean of three experiments for per parameter is used in the analysis. Standard deviations are shown with a red line, BFRP samples are shown with black color, and S2-GFRP samples are shown with red color. Conventional and climb milling directions are separately evaluated in this section. It can be seen in the Figure 6.5 that S2-GFRP has burr area higher than BFRP. Based on Figure 6.5, the HSS tools presented at all test numbers i.e. (7,8, and 9 for Uncoated), or (16,17,18 for Coated) resulted in maximum burr area.

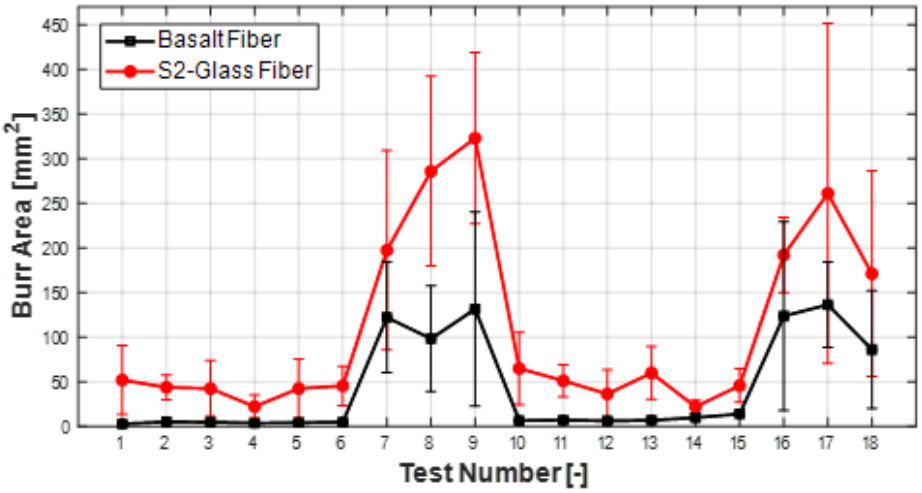

Figure 6.5 Burr area for conventional milling

Although the coating of tools does dramatically change the surface properties, it has relatively little effect on cutting quality in relation to burr area and length. The burr area of BFRP is remarkably less than S2-GFRP even with the difference in thickness. The size of the burr area is typically less with a conventional cut than climb cutting. Being more important for this text, the standard deviation in burr length and area is much greater when samples are machined with HSS, explained by formation of non-regular burrs as depicted in Figure 6.6.

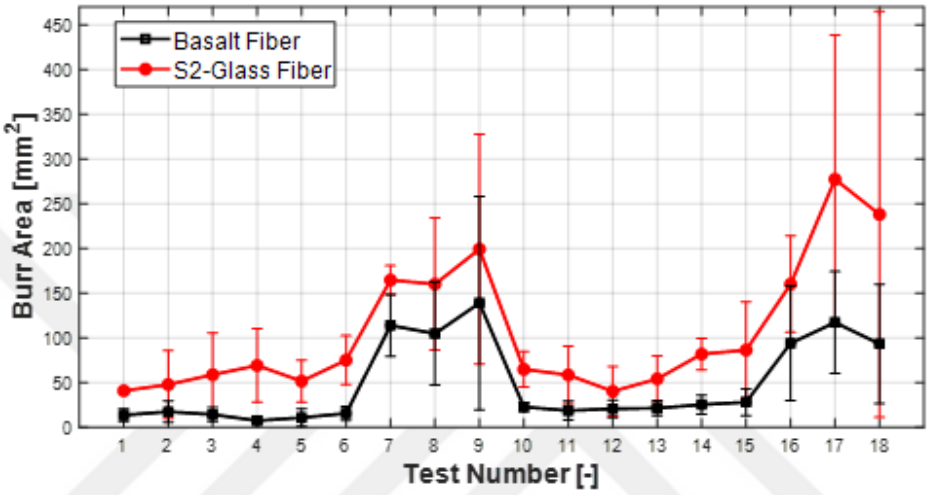

Figure 6.6 Burr area for climb milling

Climb milling of S2-Glass has a similar overall pattern compared to climb milling. HSS tools performed also poorly in the climb milling, and as expected, BFRP samples showed a low burr area compared to the S2-GFRP. One of the most important things to deduce from the comparison of Figure 6.5 and Figure 6.6 Burr area for climb milling is that the parameters for lowest and highest burr area except the HSS change with the cutting direction. For S2-GFRP Number 4 and 14 which corresponds to uncoated straight carbide with spindle speed of 500 and feed rate of 0.05 and coated straight carbide with spindle speed of 1000 and feed rate of 0.15 can be observed as the lowest burr area for S2-GFRP samples in conventional milling, however, the same experimental parameters performed significantly poor in the climb milling. Numbers 1 and 12, which correspond to uncoated helical carbide with a spindle speed of 500 and feed rate of 0.05 and coated helical carbide with a spindle speed of 1500 and feed rate of 0.1 showed exceptionally good performance with low burr area.

For BFRP samples, conventional milling performance has its optimum values on the experiments 1 and 4 that correspond to uncoated helical carbide with a spindle speed of 500 and feed rate of 0.05 and uncoated straight carbide with spindle speed of 500 and feed rate of 0.05. For climb milling the same parameters show optimum results compared to the other parameters.

Length analysis of the composite samples is done in a similar fashion. The data for the conventional burr length can be seen in Figure 6.7.

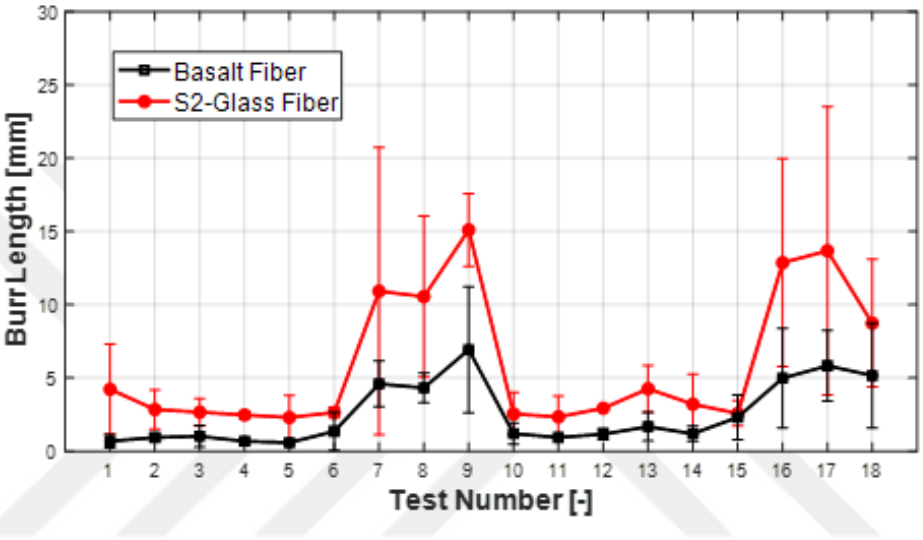

Figure 6.7 Conventional burr length of S2-GFRP and BFRP

Conventional burr length of glass fibers seemingly has the lowest values in parameter in experiment number 5 and 11, which corresponds to the parameters for uncoated straight carbide with a spindle speed of 1000 and a feed rate of 0.1 and coated helical carbide with a spindle speed of 1000 and a feed rate of 0.05. For conventional milling of BFRP, numbers 4 and 5 that corresponds to uncoated straight carbide with spindle speed of 500 and feed rate of 0.05 and uncoated straight carbide with a spindle speed of 1000 and a feed rate of 0.1. It can be observed that coated basalt samples resulted with more burr length compared to its uncoated counterparts.

Figure 6.8Figure 6.8 Climb burr length of S2-GFRP and BFRP shows that the climb milling burr length graph shows sharp peaks and relatively close lengths between S2-GFRP and BFRP. For S2-GFRP, the lowest burr length is observed in the experiments 1 and 13, which corresponds to the parameter combinations with uncoated helical carbide with a spindle speed of 500 and feed rate of 0.05 and coated straight carbide with a spindle speed of 500 and feed rate of 0.01. The graph shows that the experiments 3 and 5 shows the lowest burr for basalt, which corresponds to uncoated helical carbide with a spindle speed of 1500 and feed rate of 0.15 and uncoated straight carbide with a spindle speed of 1000 and feed rate of 0.1. The statistical significance and the effect of each parameter will be discussed in Chapter 7.

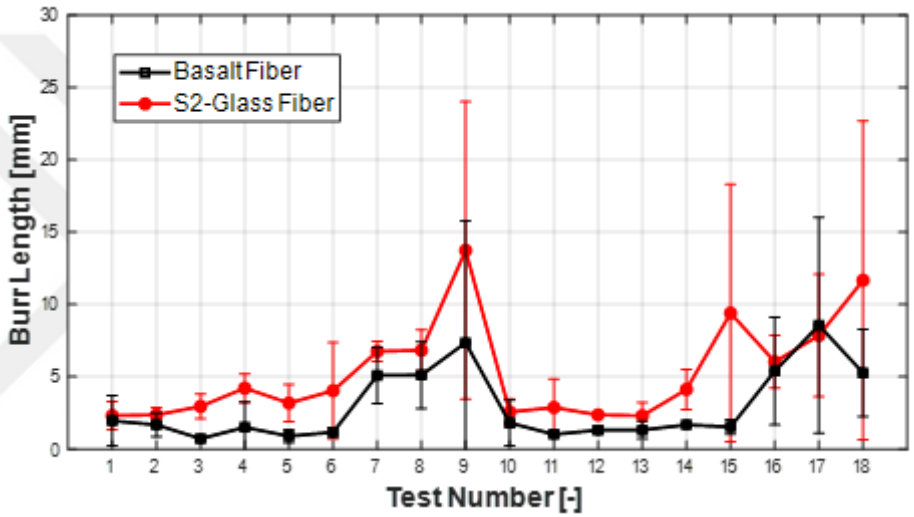

Figure 6.8 Climb burr length of S2-GFRP and BFRP

Chapter 7

Statistical Analysis

In this section, the statistical analysis of the composite samples will be explained in detail. Minitab® Statistical Software is used for data analysis for Signal-to-noise (S/N) ratio analysis and analysis of variance (ANOVA). Desirability analysis is made in MATLAB. The details to the analyses will be provided and detailed conclusions will be derived from the obtained graphs and tables.

7.1 Signal-to-Noise (S/N) Ratio Analysis

S/N ratio is a measure in Taguchi method for optimization of the process parameters by minimizing the variability caused by noise factors. The purpose of this analysis is to identify the parameter combination with the least variation due to noise. The parameter combination that varies the least can be considered as the optimum parameter for the process.

7.1.1 Introduction to S/N Ratio

The S/N ratio is based on the measured independent variables. In this study, the burr area and burr length are the resulting parameters. The desirable outcome for a sample is to have the lowest burr area and shortest burr length. S/N ratio analysis has a formulation for this specific scenario, which is the "smaller-the-better". The analysis is calculated by;

$$\frac{S}{N} = -10log10\left(\frac{1}{r}\sum_{i=1}^{r} R_i^2\right) \tag{7.1}$$

*w*here R_i^2 is the measured or observed value of the response variable -in this case it is burr area or burr length- and r is the number of observations. A high S/N ratio represents a more stable signal per noise factor, meaning less variability of the effect of parameters,

therefore desirable. S/N ratios for burr area and burr length are calculated for each combination of parameters, which are tool coating, tool geometry, spindle speed and feed rate. Since the experiment is based on three repeats of each composite sample, the mean of the three values is used in the S/N ratio calculation table.

7.1.2 Signal-to-Noise Data

S/N graphs are obtained for each material and evaluated accordingly. Burr area and burr length are shown in the same graph for better comparison. Separate graphs are presented for each cutting direction, conventional and climb. The S/N graphs for S2-GFRP can be seen in Figure 7.1. The parameter that corresponds to the higher value in S/N ratio graph is a better parameter.

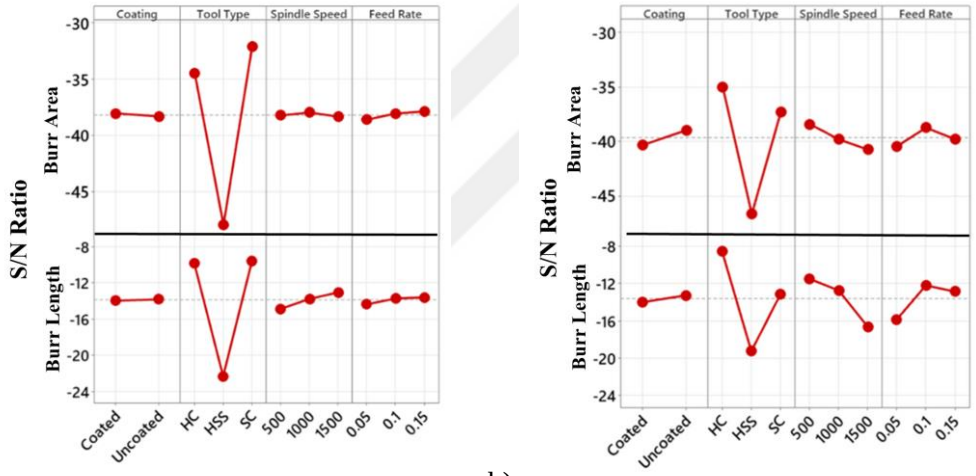

a) b)

Figure 7.1 S/N ratio graphs for Burr area and burr length for a) conventional and b) climb milling of S2-GFRP

Conventional and climb cutting methods have different optimum parameters. And although the overall trend is similar, there are differences in the burr area and burr length parameters of the same material. According to Figure 7.1a, conventional burr area shows better results with coated straight carbide with spindle speed of 1000 and feed rate of 0.15. Conventional burr length is optimum for uncoated straight carbide with spindle speed of 1500 and feed rate of 0.15. According to Figure 7.1b, climb burr area is optimum for uncoated helical carbide with a spindle speed of 500 and feed rate of 0.1, while climb burr length is optimum for uncoated helical carbide with a spindle speed of 500 and feed rate of 0.1.

The effect of coating on the response variables is insignificant for conventional milling, while it is slightly beneficial to use uncoated tools for the climb milling. The effect of high-speed steel (HSS) tools on the S/N curve is the lowest. This means that the composite samples machined with HSS tools has significantly higher burr area and burr length compared to the other tools. Different cutting directions seem to resonate better with different tool geometries. While straight carbide is optimum for the conventional milling, helical carbide is significantly better for climb milling. Spindle speed and feed rate is not significant for conventional milling, while the parameters are almost as significant as the tool type for climb milling. It is possible to conclude that lower spindle speeds work better with climb milling, while feed rate peaks at 0.1. BFRP samples showed different optimum parameter combinations for conventional and climb milling. Taguchi analysis results for BFRP samples can be seen in Figure 7.2.

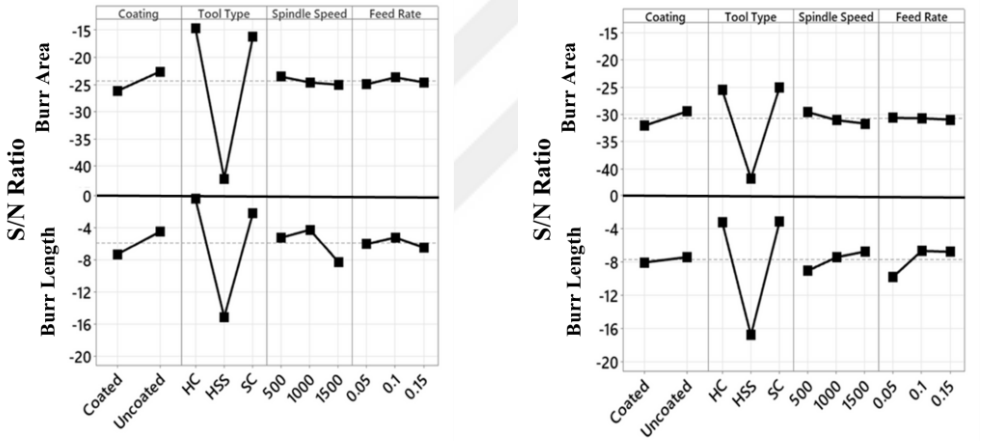

a) b)

Figure 7.2 S/N ratio graphs for Burr area and burr length for a) conventional and b) climb milling of BFRP

Similar to S2-GFRP samples, conventional and climb milling results with different optimum parameters. For conventional milling, uncoated tools showed better results compared to their coated counterpart. The tool type, similar to S2-GFRP, peaked for carbide tools regardless of the geometry, and HSS tools showed significantly worse burr area and burr length. The effect of spindle speed and feed rate is not significant for burr area for conventional milling, however the spindle speed follows a lower-is-better pattern, peaking at 500 rev/min, while feed rate peaks at 0.1 mm/rev, showing a moderate-is better pattern. Burr length for conventional milling of BFRP follows a similar pattern for the coating and tool type, uncoated tools showing better results and carbide tools dominating the HSS. Although it is not a notable difference, helical carbide tools showed better results

compared to the straight carbide tools for conventional milling for both burr area and burr length parameters, hinting that the tool geometry may have an effect on the optimum parameters. Spindle speed for burr length shows a moderate-is-better pattern, peaking at 1000 rev/min, while second best parameter can be seen as 500 rev/min, suggesting that lower spindle speed shows lower burr length compared to the higher spindle speed values. Feed rate also shows a moderate-is-better trend for burr length, like spindle speed. The statistical significance of the values will be discussed in ANOVA section in detail.

7.2 Analysis of Variance (ANOVA)

ANOVA is a statistical analysis that measures the statistical significance of the parameters of three or more groups of data. A special branch of this analysis is called One-Way ANOVA, where it measures the impact of a single independent variable on a continuous dependent variable. ANOVA analysis has key concepts to describe its parameters:

Factor: An independent variable that is used to categorize data into various groups. In this study, coating, tool type, spindle speed and feed rate are the factors.

Levels: Individual parameters that are defined by the factor. As an example, in coating factor, coated and uncoated parameters are the levels.

Response Variable: The parameter that is affected by the changes of factors and their levels. In this study, it is burr area and burr length.

ANOVA analysis is based on two hypotheses (H_0). The first hypothesis, the null hypothesis, suggests that all the data in all groups are equal, and there is no variance.

$$H_0 : \mu_1 = \mu_2 = \mu_3 = \cdots = \mu_k \tag{7.2}$$

where μ_i represents the mean of the i-th group.

The second is the alternative hypothesis (H_a) suggests that the mean of at least one group is different from the others. One-way ANOVA uses this hypothesis as a basis. ANOVA analysis suggests that the P-value (probability value) you obtain at the end of the analysis determines whether the data rejects the null hypothesis or not. A P-value

lower than 0.05 suggests that the null hypothesis is completely rejected, and the data is statistically significant. A P-Value above 0.05 indicates that there is not enough evidence in the data to reject the null hypothesis. However, The P-values between 0.05 and 0.1 is considered acceptable in some applications.

The data is extracted using Minitab statistical software. The default analysis also calculated multiple things along with P-value. The parameters and related explanations can be found below:

Degrees of Freedom: Refers to the number of independent variables minus one. For example, for coating there are two independent variables, which are coated and uncoated. Two minus one can be calculated as one, and degree of freedom for the coating parameter can be calculated as 1, and the degree of freedom for the other parameters can be calculated as 2, since the remaining parameters consist of three independent variables.

Sequential Sums of Squares (Seq SS): Quantifies the amount of variation between the parameters according to the input order.

Adjusted Sums of Squares (Adj SS): Quantifies the amount of variation between the parameters without taking the input order into account. In one-way ANOVA analysis, the Seq SS and Adj SS values are always equal.

Adjusted Mean Squares (Adj MS): Reflects the amount of variation explained by the model with taking degree of freedom into account.

F-value: Quantifies the association between the independent variables and response variable. The main function of this parameter is to calculate the P-value.

ANOVA analysis is done for two materials independently. Table 7. 1 and Table 7. 2 shows ANOVA values for the burr length and burr area of S2-GFRP respectively.

Table 7. 1 ANOVA table for the burr area of S2-GFRP

Source of Variance	DF	Seq SS	Adj SS	Adj MS	F	P
Coating	1	27	27	26.5	0.06	0.813
Tool Type	2	111259	111259	55629.7	123.42	0.000
Spindle Speed	2	1486	1486	743	1.65	0.241
Feed Rate	2	2508	2508	1253	2.78	0.110
Residual Error	10	4508	4508	450		
Total	17	119787				

ANOVA analysis in Table 7. 1 and Table 7. 2 reveals the statistical significance of independent parameters. Coating with a P-value of 0.813 is completely irrelevant to the burr area. Tool type with a P-value of 0 shows the strongest significance in all of the parameters. Spindle speed with a P-value of 0.241 is not relevant to the burr area since the P-value is above 0.1. Feed rate with a P-value of 0.110 is slightly out of range of relevance, but still considered as irrelevant.

Table 7. 2 ANOVA table for burr length of S2-GFRP

Source of Variance	DF	Seq SS	Adj SS	Adj MS	F	P
Coating	1	0.069	0.069	0.069	0.07	0.801
Tool Type	2	207.641	207.641	103.820	100.29	0.000
Spindle Speed	2	8.047	8.047	4.023	3.89	0.056
Feed Rate	2	11.071	11.071	5.535	5.35	0.026
Residual Error	10	10.352	10.352	1.035		
Total	17	237.179				

For burr length, shown in Table 7. 2 coating with a P-value of 0.801 is still out of range of relevance by far. Tool type with a P-value of 0 is still the most significant factor in the table. Spindle speed with a P-value of 0.056 is a relatively reliable parameter and influences the burr length. Feed rate with a P-value of 0.026 is strongly related to the burr length of the samples.

Table 7. 3 ANOVA analysis for the burr area of BFRP

Source of Variance	DF	Seq SS	Adj SS	Adj MS	F	P
Coating	1	8.1	8.1	8.1	0.06	0.808
Tool Type	2	40944.3	40944.3	20472.2	158.38	0.000
Spindle Speed	2	9.2	9.2	4.6	0.04	0.965
Feed Rate	2	300.1	300.1	150.1	1.16	0.352
Residual Error	10	1292.6	1292.6	129.3		
Total	17	42554.3				

Basalt samples, as expected, have different parameters that are significant to the burr area and burr length. According to Table 7. 3 for burr area, coating with a P-value of 0.808 continues to be irrelevant in the burr formation. Tool type with a P-value of 0 is also the most significant parameter in the basalt samples. Spindle speed with a P-value of 0.965 is the highest number of P-value in this analysis, therefore it is statistically insignificant. Spindle speed with a P-value of 0.352 is also statistically insignificant due to the high P-value.

Table 7. 4 ANOVA analysis for the burr length of BFRP

Source of Variance	DF	Seq SS	Adj SS	Adj MS	F	P
Coating	1	0.4622	0.4622	0.4622	1.10	0.319
Tool Type	2	79.3998	79.3998	39.6999	94.49	0.000
Spindle Speed	2	0.4081	0.4081	0.2041	0.49	0.629
Feed Rate	2	2.4912	2.4912	1.2456	2.96	0.097
Residual Error	10	4.2014	4.2014	0.4201		
Total	17	86.9628				

The burr length of basalt samples is also affected by similar parameters. It can be seen in Table 7. 4 that coating with a P-value of 0.319 is statistically insignificant due to the high value of P-value. Tool type is still the parameter that affects the burr formation in the most significant way. Spindle speed with a P-value of 0.629 is out of range of relevance, while feed rate with a P-value of 0.097 is barely inside the range that could be considered as relevant. In every single ANOVA analysis, coating is consistently statistically insignificant while tool type with a P-value of 0.000 in all cases is the most

statistically significant parameter. Spindle speed and feed rate, while not being significant for the burr area calculations, is an important parameter for burr length for the most cases.

7.3 Desirability Analysis

Desirability analysis is an analysis when the comparison of two parameters is required. In this case, material removal rate (MRR) is considered as a positive parameter, while the burr area is considered as the negative parameter. It is expected from a sample to have a high MRR, since it corresponds to faster operation time, and higher applicability in the industry. Low spindle speed and feed rate may result in lower burr quality, however, for example, if 5 samples could be machined during the same time, it wouldn't be a profitable parameter for the CNC owner. Therefore, in order to connect this academic endeavor to the industry, a desirability analysis is conducted. MRR is calculated for every parameter. The resulting table can be seen Table 7. 5.

Table 7. 5 MRR with respect to the Taguchi parameter combinations

Test #	Tool Surface	Tool Type	Spindle speed	Feed rate	MRR [mm³/min]	
					S2-GFRP	BFRP
1	1	1	1	1	169	225
2	1	1	2	2	675	900
3	1	1	3	3	1519	2026
4	1	2	1	1	169	225
5	1	2	2	2	675	900
6	1	2	3	3	1519	2026
7	1	3	1	2	338	450
8	1	3	2	3	1013	1350
9	1	3	3	1	506	676
10	2	1	1	3	506	676
11	2	1	2	1	338	450
12	2	1	3	2	1013	1350
13	2	2	1	2	338	450
14	2	2	2	3	1013	1350
15	2	2	3	1	506	676
16	2	3	1	3	506	676
17	2	3	2	1	338	450
18	2	3	3	2	1013	1350

Since the burr areas are known from the previous chapters The desirability of each parameter can be calculated according to the formula:

$$D = \sqrt{(d_{burr} * d_{MRR})} \tag{7.2}$$

Where d_{burr} and d_{MRR} corresponding to the individual desirability of the parameters. High MRR and low burr area is defined as desirable, therefore it can be calculated as:

$$d_{MRR} = \frac{x - \min(X)}{\max(X) - \min(X)} \tag{7.3}$$

$$d_{burr} = 1 - \frac{x - \min(X)}{\max(X) - \min(X)} \tag{7.4}$$

The resulting table after calculating the individual and composite desirability of the parameters can be seen in Table 7.7: Individual and composite desirability of the parameters for BFRP .

Table 7. 6 and Table 7.7: Individual and composite desirability of the parameters for BFRP .

Table 7. 6: Individual and composite desirability of the parameters for S2-GFRP

Material	**S2-GFRP**					
Direction	**Conventional**			**Climb**		
Desirability	d_{Burr}	d_{MRR}	D	d_{Burr}	d_{MRR}	D
1	0.900	0.000	0.000	0.998	0.000	0.000
2	0.927	0.375	0.590	0.969	0.375	0.602
3	**0.932**	**1.000**	**0.965**	**0.922**	**1.000**	**0.960**
4	0.999	0.000	0.000	0.878	0.000	0.000
5	0.932	0.375	0.591	0.952	0.375	0.597
6	**0.922**	**1.000**	**0.960**	**0.853**	**1.000**	**0.924**
7	0.417	0.125	0.229	0.475	0.125	0.244
8	0.123	0.625	0.278	0.495	0.625	0.556
9	0.000	0.250	0.000	0.330	0.250	0.287
10	0.857	0.250	0.463	0.896	0.250	0.473
11	0.903	0.125	0.336	0.923	0.125	0.340
12	0.952	0.625	0.772	1.000	0.625	0.791
13	0.874	0.125	0.331	0.942	0.125	0.343
14	1.000	0.625	0.791	0.824	0.625	0.718
15	0.921	0.250	0.480	0.806	0.250	0.448
16	0.435	0.250	0.330	0.495	0.250	0.351
17	0.206	0.125	0.161	0.000	0.125	0.000
18	0.505	0.625	0.562	0.166	0.625	0.322

It can be seen from Table 7. 6 that the experiment number 3 and 6 shows the highest desirability with the composite desirability values of 0.965 and 0.960 for conventional,

and 0.960 and 0.924 for climb for S2-GFRP highlighted in bold. Similarly, for BFRP in Table 7.7: Individual and composite desirability of the parameters for BFRP10, experiment number 3 and 6 with the composite desirability of 0.993 and 0.993 for conventional and 0.974 and 0.969 for climb milling showed the most desirable outcomes. Although they are not the optimum burr area parameters in some cases, they possess the highest MRR with the combination of highest spindle speed of 1500 and highest feed rate of 0.15. Composite desirability calculation weighs the MRR and burr area equally, therefore the lowest burr area parameters such as 4 and 14 show significantly desirability due to the low MRR.

Table 7.7: Individual and composite desirability of the parameters for BFRP

Material	**BFRP**					
Direction	**Conventional**			**Climb**		
Desirability	d_{Burr}	d_{MRR}	D	d_{Burr}	d_{MRR}	D
1	1.000	0.000	0.000	0.953	0.000	0.000
2	0.983	0.375	0.607	0.923	0.375	0.588
3	**0.985**	**1.000**	**0.993**	**0.948**	**1.000**	**0.974**
4	0.993	0.000	0.000	1.000	0.000	0.000
5	0.990	0.375	0.609	0.974	0.375	0.604
6	**0.985**	**1.000**	**0.993**	**0.938**	**1.000**	**0.969**
7	0.106	0.125	0.115	0.190	0.125	0.154
8	0.285	0.625	0.422	0.260	0.625	0.403
9	0.037	0.250	0.096	0.000	0.250	0.000
10	0.972	0.250	0.493	0.883	0.250	0.470
11	0.968	0.125	0.348	0.915	0.125	0.338
12	0.974	0.625	0.780	0.899	0.625	0.749
13	0.970	0.125	0.348	0.894	0.125	0.334
14	0.947	0.625	0.769	0.864	0.625	0.735
15	0.916	0.250	0.479	0.843	0.250	0.459
16	0.095	0.250	0.155	0.342	0.250	0.293
17	0.000	0.125	0.000	0.165	0.125	0.143
18	0.376	0.625	0.485	0.347	0.625	0.466

It is also important to note that the optimum value of desirability is the same for both BFRP and S2-GFRP samples, regardless of the optimum parameter difference of the burr area. The weight of MRR and burr area in the equation can be mathematically arranged to be tailored for specific applications. For example, the weight of the MRR could be increased for the applications that would require faster operations while the weight of the burr area could be increased for more sensitive applications.

Chapter 8

Conclusions and Future Prospects

8.1 Conclusions

The vacuum infusion method used in the production processes of S2-GFRP and BFRP composites offers significant advantages in terms of sustainability. This method provides an environmentally friendly production process with low energy consumption and minimal waste production. Additionally, the recyclability of the materials used reduces environmental impacts and contributes to sustainable production goals.

In this study, analysis of damages occurring during the processing of S2-GFRP and BFRP composites is of great importance in terms of sustainability. Minimizing damage occurring during the processing process reduces material waste and increases production efficiency. This provides both economic and environmental benefits. Additionally, acoustic emission techniques used for damage analysis are faster and less invasive than traditional damage detection methods. This contributes to sustainable production processes by saving energy and resources.

The use of composite materials reduces carbon footprint by increasing fuel efficiency in sectors such as automotive and aviation. S2-GFRP and BFRP composites offer lighter and more durable solutions compared to traditional materials in these sectors. This means less fuel consumption in vehicles and therefore lower carbon emissions. Additionally, the longevity of these composites extends the lifespan of vehicles, reducing the need for frequent maintenance and replacement.

In conclusion, the S2-GFRP and BFRP composite materials examined in this study offer various advantages in terms of sustainability. With their energy and material savings in production processes, environmental durability and recyclability, these composites offer sustainable solutions in modern engineering applications. In this context, the use of such advanced materials and optimizing processing techniques are of great importance to achieve sustainability goals.

8.2 Societal Impact and Contribution to Global Sustainability

Sustainability is becoming increasingly important in modern engineering and manufacturing processes. S2-GFRP and BFRP composites discussed in this study offer important contributions to sustainability. These composite materials attract attention with their high mechanical strength, low density and environmental durability. Optimizing the machining parameters for those materials decrease the amount of material that is wasted due to rejection of parts and potentially elongate the service life of the composite materials. The reduction of waste also conserves the raw materials and saves energy by eliminating or decreasing the energy required for the post-processing of the materials.

A desirability analysis is conducted to optimize the machining process for industrial applications. An increase in desirability results with a decreased operation time with a small amount of sacrifice from the burr area and burr length. Faster operation time corresponds to less time and energy spent by the lathes and people in the industry.

Basalt fibers are natural fibers that are obtained from volcanic rocks and are considered as an environmentally friendly alternative to synthetic fibers such as glass. The strength and elastic modulus of BFRP is, although slightly inferior, comparable to

S2-GFRP. The optimization efforts presented in the study are expected to increase the utilization of BFRP in the industry, decreasing the long-term environmental footprint of the composite materials.

Another point that is suggested by the research is the inefficiency of the coating process. Vacuum process and magnetron sputtering uses high amount of electricity during the coating of the tools. The process also uses titanium as target material, and various gases as a source of plasma. By decreasing the efforts for coating the tools, it is possible to save significant amounts of energy, raw materials and time. However, the tool life is not observed in this study. It is possible that coating the tools with thin-film coatings increase the service life of the tools. Further research on this topic may further increase the sustainability and energy efficiency of composite milling.

8.3 Future Prospects

In future research, several important studies are recommended to better understand the performance and durability of composite materials. These studies include performing fatigue tests on S2-Glass Fiber Reinforced Polymer (S2-GFRP) and Basalt Fiber Reinforced Polymer (BFRP) samples in accordance with ASTM 3039 standards. ASTM 3039 standards contain testing procedures used to determine the tensile properties of polymer matrix composite materials. Fatigue tests to be carried out in accordance with these standards will simulate the mechanical stresses that S2-GFRP and BFRP materials will be exposed to under cyclic loading conditions and evaluate the long-term performance and durability of these materials. Test results will determine the effects of fatigue on the material and provide important data to consider in material design and applications.

Additionally, acoustic emission tests were carried out for damage analysis. Acoustic emission technique is an effective method for early detection and monitoring of damage to materials. This technique involves detecting and analyzing acoustic waves created by

damaging events such as microcracks, fiber breaks and matrix separations that occur within the material. Acoustic emission sensors are placed on the surface of the material and record these waves, helping to determine the location, type and extent of damage. These experiments will provide valuable information about the structural integrity of S2-GFRP and BFRP materials and provide important data to improve the reliability and effectiveness of these materials in engineering applications. Processing the acoustic emission data along with the fatigue experiments may reveal a correlation between the burr area and the fatigue strength of composite materials.

These comprehensive studies aim to ensure that composite materials are more reliable and durable in engineering applications and will contribute to expanding the potential areas of use of these materials.

This project is sponsored within the framework of TUBITAK 1001 with the project code 221M085.

BIBLIOGRAPHY

[1] E. Kılıçkap, A. Yardımeden, and Y. H. Çelik, "Investigation of Experimental Study of End Milling of CFRP Composite," *Science and Engineering of Composite Materials*, 2015, doi: 10.1515/secm-2013-0143.

[2] K. Palanikumar, T. N. Srinivasan, K. Rajagopal, and J. P. Davim, "6. Drilling of High Impact Polystyrene Composites Materials," 2015, doi: 10.1515/9783110292251-007.

[3] Y. N. Jurn, S. A. Mahmood, Qasim Habeeb, and Imad, "Performance Prediction of Bundle Double-Walled Carbon Nanotube-Composite Materials for Dipole Antennas at Terahertz Frequency Range," *Progress in Electromagnetics Research M*, 2020, doi: 10.2528/pierm19101604.

[4] C. YILDIRIM, E. TURGUT, S. SÜRDEM, and A. Yörükoğlu, "Investigating the Effect of Drawing Process Parameters on Borosilicate Glass Fiber Thickness," *Journal of Boron*, 2022, doi: 10.30728/boron.953341.

[5] J. Skoczylas, S. Samborski, and M. Kłonica, "The Application of Composite Materials in the Aerospace Industry," *Journal of Technology and Exploitation in Mechanical Engineering*, 2019, doi: 10.35784/jteme.73.

[6] J. Hong, C. Hu, L. Jin, X. Han, J. Yao, and I. Gil, "Conductive Polyaniline-Coated Poly(p-Phenylenetere Phthamide) Yarn-Reinforced Multiaxial Composites for Electromagnetic Shielding," *Journal of Industrial Textiles*, 2019, doi: 10.1177/1528083719883048.

[7] U. Nirmal, "A Review on Tribological Performance of Polymeric Composites Based on Natural Fibres," 2018, doi: 10.21741/9781945291876-10.

[8] E. Ünal, "Temperature and Thrust Force Analysis on Drilling of Glass Fiber Reinforced Plastics," *Thermal Science*, 2019, doi: 10.2298/tsci180117181u.

[9] Y. Qiao, O. Das, S. Zhao, T. Sun, Q. Xu, and L. Jiang, "Pyrolysis Kinetic Study and Reaction Mechanism of Epoxy Glass Fiber Reinforced Plastic by Thermogravimetric Analyzer (TG) and TG–FTIR (Fourier-Transform Infrared) Techniques," *Polymers (Basel)*, 2020, doi: 10.3390/polym12112739.

[10] V. La Carrubba, M. Bulters, and W. Zoetelief, "Dependence of Coefficient of Volumetric Thermal Expansion (CVTE) of Glass Fiber Reinforced (GFR) Polymers on the Glass Fiber Content," *Polymer Bulletin*, 2007, doi: 10.1007/s00289-007-0819-0.

[11] K. S. Lee *et al.*, “A Study on Optimizing the Mechanical Properties of Glass Fiber-Reinforced Polypropylene for Automotive Parts,” *Polym Plast Technol Eng*, 2011, doi: 10.1080/03602559.2010.531417.

[12] T. Mayr, F. Niedermeier, and M. Hassler, “Application of Composite Materials in Inductive Charging Systems for Electric Vehicles,” *J Compos Mater*, 2019, doi: 10.1177/0021998318824637.

[13] R. M. Thomsen, S. F. Garzón, D. Herfort, and Y. Yue, “Physical Performances of Alkali-activated Portland Cement-glass-limestone Blends,” *Journal of the American Ceramic Society*, 2017, doi: 10.1111/jace.14955.

[14] K. Kanehara, S. Urata, S. Yasuhara, T. Tsurumi, and T. Hoshina, “Dielectric Response and Polarization Mechanism of Alkali Silicate Glasses in Gigahertz to Terahertz Frequency Range,” *Journal of the American Ceramic Society*, 2023, doi: 10.1111/jace.19189.

[15] D. Di Martino, L. F. Santos, R. M. Almeida, and M. F. Montemor, “X-ray Photoelectron Spectroscopy of Alkali Germanate Glasses,” *Surface and Interface Analysis*, 2002, doi: 10.1002/sia.1310.

[16] S. Ghosh and A. Ghosh, “Mixed Mobile Ion Effect in Fluorozincate Glasses,” *Journal of Physics Condensed Matter*, 2005, doi: 10.1088/0953-8984/17/23/001.

[17] K. A. Krishnan, R. Anjana, and K. E. George, “Effect of Alkali-resistant Glass Fiber on Polypropylene/Polystyrene Blends: Modeling and Characterization,” *Polym Compos*, 2014, doi: 10.1002/pc.23193.

[18] M. A. Boumehraz, M. Mellas, K. Goudjil, and F. Boucetta, “Study of the Aging of a Concrete Reinforced by Alkali Resistant Glass Fiber in the Wet Environment,” *Annales De Chimie Science Des Matériaux*, 2020, doi: 10.18280/acsm.440202.

[19] M. Hasanuzzaman, M. Sajjia, A. Rafferty, and A.-G. Olabi, “Thermal Behaviour of Zircon/Zirconia-Added Chemically Durable Borosilicate Porous Glass,” *Thermochim Acta*, 2013, doi: 10.1016/j.tca.2012.12.018.

[20] P. Ma *et al.*, “Facile Synthesis of Novel Dopamine-Modified Glass Fibers for Improving Alkali Resistance of Fibers and Flexural Strength of Fiber-Reinforced Cement,” *RSC Adv*, 2021, doi: 10.1039/d1ra01875b.

[21] J. Anjaiah, “Impact of Rare-Earth Ion Doping on Dielectric Properties of Li₂O-CaO-B₂O₃ Glass System,” *Ecs Journal of Solid State Science and Technology*, 2022, doi: 10.1149/2162-8777/ac95c8.

[22] K. Kanehara, S. Urata, S. Yasuhara, T. Tsurumi, and T. Hoshina, “Dielectric Property and Polarization Mechanism of Sodium Silicate Glass in GHz–THz Range,” *Jpn J Appl Phys*, 2022, doi: 10.35848/1347-4065/ac7b0f.

[23] P. Bhuyan *et al.*, “Development of Cu-E-Glass Fiber Composites by Powder Metallurgy Route,” *IOP Conf Ser Mater Sci Eng*, 2016, doi: 10.1088/1757-899x/115/1/012023.

[24] Y. Yuan, H.-I. Lin, Z. Jiang, Z. Chi, M. Yao, and S. Zhang, “Effects of Content of Chopped Glass Fibers on the Properties of Silica Filled PTFE Composites,” *Journal of Materials Science and Chemical Engineering*, 2017, doi: 10.4236/msce.2017.57005.

[25] D. Prabu and Tjprc, “A Review on Mechanical Properties of Intra-Layer Palm Fiber (Palmyra Spout) - Flax - S-Glass Fiber Reinforced Composite,” *International Journal of Mechanical and Production Engineering Research and Development*, 2018, doi: 10.24247/ijmperdjun201853.

[26] K. H. Cho *et al.*, “Influence of Surface Treatment on the Interfacial and Mechanical Properties of Short S-Glass Fiber-Reinforced Dental Composites,” *ACS Appl Mater Interfaces*, 2019, doi: 10.1021/acsami.9b01857.

[27] U. Vaidya, M. Kulkarni, M. Hosur, A. Mayer, and P. K. Dutta, “High Strain Rate Response of S2-Glass/Epoxy Composites With Polycarbonate Facing,” *Polymers and Polymer Composites*, 2001, doi: 10.1177/096739110100900201.

[28] J. Qiu, C. Zhang, B. Wang, and R. Liang, “Carbon nanotube integrated multifunctional multiscale composites,” *Nanotechnology*, vol. 18, no. 27, 2007, doi: 10.1088/0957-4484/18/27/275708.

[29] A. Dogan and N. Karaca, “Experimental and theoretical behavior of cementitious plates containing ethylene vinyl acetate reinforced with glass woven fabric under impact load,” *Materials Science- Poland*, vol. 39, no. 4, pp. 491–506, 2021, doi: 10.2478/msp-2021-0041.

[30] V. Fiore and L. Calabrese, “Effect of stacking sequence and sodium bicarbonate treatment on quasi-static and dynamic mechanical properties of flax/jute epoxy-based composites,” *Materials*, vol. 12, no. 9, 2019, doi: 10.3390/ma12091363.

[31] M. R. Ricciardi *et al.*, “A New Cost-Saving Vacuum Infusion Process for Fiber-Reinforced Composites: Pulsed Infusion,” *J Compos Mater*, 2013, doi: 10.1177/0021998313485998.

[32] A. R. Mills and J. G. Jones, “Investigation, Manufacture, and Testing of Damage-Resistant Airframe Structures Using Low-Cost Carbon Fibre Composite Materials and Manufacturing Technology,” *Proc Inst Mech Eng G J Aerosp Eng*, 2010, doi: 10.1243/09544100jaero573.

[33] A. A. Talabari, M. H. Alaei, and H. Shalian, “Experimental Investigation of Tensile Properties in a Glass/Epoxy Sample Manufactured by Vacuum

Infusion, Vacuum Bag and Hand Layup Process," *Revue Des Composites Et Des Matériaux Avancés*, 2019, doi: 10.18280/rcma.290308.

[34] K. I. Rana, Z. Sajid, J. Tao, and L. A. Khan, "Effect of Vacuum Manipulation on Inter Laminar Shear Strength and Flexural Strength in Double Bag Vacuum Infusion Moulding," *Polymers and Polymer Composites*, 2021, doi: 10.1177/09673911211004206.

[35] A. Köpf, S. Feistritzer, and K. Udier, "Diamond coated cutting tools for machining of non-ferrous metals and fibre reinforced polymers," *Int J Refract Metals Hard Mater*, vol. 24, no. 5, pp. 354–359, 2006, doi: 10.1016/j.ijrmhm.2005.11.013.

[36] P. J. Kelly, J. Hisek, Y. Zhou, R. D. Pilkington, and R. D. Arnell, "Advanced coatings through pulsed magnetron sputtering," *Surface Engineering*, vol. 20, no. 3, pp. 157–162, 2004, doi: 10.1179/026708404225010702.

[37] R. Haubner, M. Lessiak, R. Pitonak, A. Köpf, and R. Weissenbacher, "Evolution of conventional hard coatings for its use on cutting tools," *Int J Refract Metals Hard Mater*, vol. 62, no. January 2017, pp. 210–218, 2017, doi: 10.1016/j.ijrmhm.2016.05.009.

[38] S. Atta, U. NarendraKumar, K. V. A. N. P. S. Kumar, D. P. Yadav, and S. Dash, "Recent Developments and Applications of TiN-Based Films Synthesized by Magnetron Sputtering," *J Mater Eng Perform*, vol. 32, no. 22, pp. 9979–10015, 2023, doi: 10.1007/s11665-023-08273-x.

[39] A. Z. Ait Djafer, N. Saoula, N. Madaoui, and A. Zerizer, "Deposition and characterization of titanium carbide thin films by magnetron sputtering using Ti and TiC targets," *Appl Surf Sci*, vol. 312, no. May, pp. 57–62, 2014, doi: 10.1016/j.apsusc.2014.05.084.

[40] A. Knap, Š. Dvořáčková, and T. Knápek, "Study of the Machining Process of GFRP Materials by Milling Technology with Coated Tools," *Coatings*, vol. 12, no. 9, 2022, doi: 10.3390/coatings12091354.

[41] A. Mkaddem, A. Soussia, and M. EL Mansori, "Wear resistance of CVD and PVD multilayer coatings when dry cutting fiber reinforced polymers (FRP)," *Wear*, vol. 302, pp. 946–954, Apr. 2013, doi: 10.1016/j.wear.2013.03.017.

[42] K. Colligan and M. Ramulu, "Delamination in surface plies of graphite\epoxy caused by the edge trimming process," *Processing and Manufacturing of Composite Materials*, vol. 27, no. JANUARY 1991, pp. 113–125, 1991.

[43] T. Gao *et al.*, *Fiber-reinforced composites in milling and grinding: machining bottlenecks and advanced strategies*, vol. 17, no. 2. 2022. doi: 10.1007/s11465-022-0680-8.

[44] P. M. M. S. Sarma, L. Karunamoorthy, and K. Palanikumar, “Modeling and analysis of cutting force in turning of GFRP composites by CBN tools,” *Journal of Reinforced Plastics and Composites*, vol. 27, no. 7, pp. 711–723, 2008, doi: 10.1177/0731684407084214.

[45] H. Hocheng and C. C. Tsao, “Effects of special drill bits on drilling-induced delamination of composite materials,” *Int J Mach Tools Manuf*, vol. 46, no. 12–13, pp. 1403–1416, 2006, doi: 10.1016/j.ijmachtools.2005.10.004.

[46] M. P. Jenarthanan, A. Prakash, and R. Jeyapaul, “Mathematical Modeling of Delamination Factor on End Milling of Hybrid GFRP Composites Through RSM,” *Pigment \& Resin Technology*, 2016, doi: 10.1108/prt-08-2015-0083.

[47] E. Kilickap, “Analysis and modeling of delamination factor in drilling glass fiber reinforced plastic using response surface methodology,” *J Compos Mater*, vol. 45, no. 6, pp. 727–736, 2011, doi: 10.1177/0021998310381539.

[48] R. Stone and K. Krishnamurthy, “A neural network thrust force controller to minimize delamination during drilling of graphite-epoxy laminates,” *Int J Mach Tools Manuf*, vol. 36, no. 9, pp. 985–1003, 1996, doi: 10.1016/0890-6955(96)00013-2.

[49] D. Nayak, N. Bhatnagar, and P. Mahajan, “Machining studies of Uni-Directional Glass Fiber Reinforced Plastic (UD-GFRP) composites part 1: Effect of geometrical and process parameters,” *Machining Science and Technology*, vol. 9, no. 4, pp. 481–501, 2005, doi: 10.1080/10910340500398167.

[50] P. Masek, P. Zeman, P. Kolar, and F. Holesovsky, “Edge trimming of C/PPS plates,” *International Journal of Advanced Manufacturing Technology*, vol. 101, no. 1–4, pp. 157–170, 2019, doi: 10.1007/s00170-018-2857-1.

[51] F. Ceritbinmez, A. Yapici, and E. Kanca, “The Effect of Nanoparticle Additive on Surface Milling in Glass Fiber Reinforced Composite Structures,” *Polymers and Polymer Composites*, 2021, doi: 10.1177/09673911211014172.

[52] S.-Y. Chun, “A Comparative Study of Superhard TiN Coatings Deposited by DC and Inductively Coupled Plasma Magnetron Sputtering,” *Journal of the Korean institute of surface engineering*, vol. 46, no. 2, pp. 55–60, 2013, doi: 10.5695/jkise.2013.46.2.055.

[53] S. Savaş and Ş. Danişman, “Multipass Sliding Wear Behavior of TiAlN Coatings Using a Spherical Indenter: Effect of Coating Parameters and Duplex Treatment,” *Tribology Transactions*, vol. 57, no. 2, pp. 242–255, 2014, doi: 10.1080/10402004.2013.868564.

[54] Ş. Danışman, D. Odabaş, and M. Teber, “The Effect of TiN, TiAlN, TiCN Thin Films Obtained by Reactive Magnetron Sputtering Method on the Wear

Behavior of Ti6Al4V Alloy: A Comparative Study," *Coatings*, vol. 12, no. 9, 2022, doi: 10.3390/coatings12091238.

[55] H. Çalişkan, C. Kurbanoğlu, P. Panjan, M. Čekada, and D. Kramar, "Wear behavior and cutting performance of nanostructured hard coatings on cemented carbide cutting tools in hard milling," *Tribol Int*, vol. 62, pp. 215–222, 2013, doi: 10.1016/j.triboint.2013.02.035.

[56] D. Ozkan, P. Panjan, M. S. Gok, and A. C. Karaoglanli, "Investigation of machining parameters that affects surface roughness and cutting forces in milling of CFRPs with TiAlN and TiN coated carbide cutting tools," *Mater Res Express*, vol. 6, no. 9, p. 95616, 2019, doi: 10.1088/2053-1591/ab30de.

[57] J. L. H. Wang J. Sun and W. Li, "Roughness modelling analysis for milling of carbon fibre reinforced polymer composites," *Materials Technology*, vol. 30, no. sup1, pp. A46--A50, 2015, doi: 10.1179/1753555715Y.0000000002.

CURRICULUM VITAE

2016-2021	B.Sc., Mechanical Engineering, Abdullah Gül University, Kayseri/Turkiye
2019	Research Intern, Kyushu University, Fukuoka/Japan
2022	Research Intern, Leibniz University of Hannover, Hannover/Germany
2022-Present	M.Sc., Advanced Materials and Nanotechnology, Abdullah Gül University, Kayseri/Turkiye

SELECTED PUBLICATIONS AND PRESENTATIONS

Sayin AC, Danisman S, Ersoy E, Yilmaz C, Kesriklioglu S. Experimental and statistical damage analysis in milling of S2-glass fiber/epoxy and basalt fiber/epoxy composites. *Polym Compos*. (2024); 1-19. doi:10.1002/pc.28826